

## Article

# Chemical and Textural Peculiarities of Zircon from Peralkaline Granites and Quartz-Bearing Syenites

Karel Breiter<sup>1,2,\*</sup> , Jindřich Kynický<sup>1</sup> and Zuzana Korbelová<sup>2</sup><sup>1</sup> BIC Brno Ltd., Purkyňova 125, CZ-61200 Brno, Czech Republic; jindrak@email.cz<sup>2</sup> Institute of Geology, Czech Academy of Sciences, Rozvojová 269, CZ-16500 Praha, Czech Republic; korbelova@gli.cas.cz

\* Correspondence: breiter@gli.cas.cz

**Abstract:** Zircon from four plutons of peralkaline granites and quartz-bearing syenites, differing in geotectonic positions, petrological and mineralogical compositions, and contents of volatile and trace elements, was studied using SEM, CL, and EPMA with the intention to define typical textural and chemical features of zircon from peralkaline rocks. In strongly peralkaline Na-pyroxene-bearing rocks represented by the Khan Bogd and Khalzan Buregte plutons (Mongolia), the primary zircon is scarce or missing. Most zircon grains are secondary, originating in hydrothermal stage from primary Zr silicates. They often form globular or radial aggregates. Chemical compositions of zircon in these rocks typically show high contents of Y, moderate contents of REE (thus high Y/Yb values) together with low contents of U and Th and low analytical totals. In mildly peralkaline mica-bearing rocks represented by Ivigtut stock (Groenland) and Madeira pluton (Brazil), the exclusive primary Zr mineral is zircon, mostly of orthomagmatic origin. Its analytical totals approach 100 wt%, enrichment in HREE, resulting in low Y/Yb values, is typical. Zircon populations from two types of peralkaline granitoids can be distinguished from each other and from zircon from S-type granites based on combination of the Zr/Hf, Y/Yb, and U/Th values, or on the Y-Hf-P ternary diagram.

**Keywords:** peralkaline rocks; zircon chemistry; Khan Bogd; Khalzan Buregte; Ivigtut; Madeira



**Citation:** Breiter, K.; Kynický, J.; Korbelová, Z. Chemical and Textural Peculiarities of Zircon from Peralkaline Granites and Quartz-Bearing Syenites. *Minerals* **2024**, *14*, 187. <https://doi.org/10.3390/min14020187>

Academic Editor: Urs Klötzli

Received: 3 January 2024

Revised: 2 February 2024

Accepted: 7 February 2024

Published: 10 February 2024



**Copyright:** © 2024 by the authors. Licensee MDPI, Basel, Switzerland. This article is an open access article distributed under the terms and conditions of the Creative Commons Attribution (CC BY) license (<https://creativecommons.org/licenses/by/4.0/>).

## 1. Introduction

Zircon is a widely distributed accessory mineral in granitic and syenitic igneous rocks; it is a fairly common detrital mineral in some sediments, and is also found in metamorphic rocks [1–3]. For its stability across a broad range of pT conditions and mineral–fluid interactions, zircon serves as a useful subject of several types of geochronological studies (review in [4]), as a geothermometer [5], or as a subject of provenance studies of clastic sediments [6]. Lu–Hf and Sm–Nd isotope systems in zircon [7,8] provide information on source lithologies of igneous complexes. Apart from all the above information potentially hidden in zircon, the shapes of zircon crystals [9] and trace-element spectra of igneous zircon [10–16] indicate geotectonic affiliation and grade of fractionation of magmatic suites. Zircon/melt partition coefficients of REE, Y, Th, U, etc., were studied by Nardi et al. [17], and those for more than 40 minor and trace elements by Padilla and Gualda [18]. Chemical changes during hydrothermal alteration of primary zircon were studied, for example, by Bell et al. [19] and Kubeš et al. [20], and the difference between associated magmatic and hydrothermal zircons was explored by Vlach [21].

Chemical compositions of zircon from common calc-alkaline granites, strongly peraluminous P-rich S-type granites, and mildly peraluminous P-poor A-type granites have been well constrained [10–12,15,16,22–26]. Because of the chemical similarity of elements Zr and Hf, mineral zircon always contains some Hf. The contents of Hf in zircon is almost the same in rocks ranging from kimberlites to common granites (0.8–1.7 wt% HfO<sub>2</sub>) and increases significantly only in strongly fractionated granites [10,27]. Hafnon, the Hf-dominant member

of the zircon group, has been found in some rare-metal pegmatites [28,29]. Among other elements, especially the contents of Y, REE, Th, U, and P reach units of wt%, in extreme cases even exceed 10 wt%, forming transitional zircon–xenotime and zircon–thorite/coffinite series [16,30,31].

Although some alkaline rocks are rich in zircon, reaching the level of potentially economically interesting mineralization [32–36], trace-element analyses of zircon from these rocks are less common. Zircons from peralkaline granitoids contain lower amounts of trace elements in general. In their pioneering work about zircon chemistry, Belousova et al. [10] referred only to a sample from nepheline syenite from southern Norway with medians of 1.46 wt% Hf, 0.25 wt% Th, 1.3 wt% Y, and 0.4 wt% Yb. Smith et al. [37] reported Hf-poor (<0.30 wt% HfO<sub>2</sub>) but Nb-enriched (up to 6.62 wt% Nb<sub>2</sub>O<sub>5</sub>) zircon from the Thor Lake alkali syenite. Pupin [11] analyzed a large number of zircon samples but reported only Hf and Y values: zircon from hypersolvus peralkaline granitoids tend to be relatively rich in Y and poor in Hf, and that from subsolvus granitoids shows the opposite. In peralkaline granites from eastern coastal China, Xie et al. [38] distinguished two types of zircon: early crystallized Th-rich zircon (1–10 wt% ThO<sub>2</sub>) and late recrystallized Th-poor zircon (<1 wt% ThO<sub>2</sub>) with thorite microinclusions. Sheard et al. [33] reported Hf-poor (<1.5 wt% HfO<sub>2</sub>), but Nb-rich (max. 2 wt% Nb<sub>2</sub>O<sub>5</sub>) and F-rich (max. 1 wt% F) zircon from the Zr–Nb–REE-enriched Thor Lake syenite, while Gysi et al. [35] found high contents of Y and HREE (usually 3–5 wt% Y<sub>2</sub>O<sub>3</sub> and max. more than 2 wt% Yb<sub>2</sub>O<sub>3</sub>) in zircon from the REE–Zr–Nb-mineralized Strange Lake peralkaline granite. Nardi et al. [39] analyzed zircons from several varieties of A-type granites of the Pitinga tin province of Brazil, including the peralkaline Madeira albite granite, and found that the latter contained the relative highest amounts of HfO<sub>2</sub> (1.8–5.0 wt%), Nb (8–825 ppm), Th (200–6649 ppm), U (456–2975 ppm), and Y (2003–9211 ppm). The reasons for the LREE enrichment of some zircons in sub- and peralkaline granites and syenites of southern Brazil were discussed by Vilalva et al. [40].

With the intention of supplementing the hitherto fragmentary data on the chemistry of zircon from peralkaline granitoids and making their general comparison with zircon chemistries from other types of granitoids, four plutons of peralkaline granitoids of different geotectonic positions, different petrological and mineral composition and different contents of volatile and trace elements were selected for a detailed study. The purpose of this paper is to compare the appearances of zircon crystals and aggregates, and to demonstrate the contents of minor and trace elements in zircon based on sufficiently large sets of analytical data, also defining basic chemical features distinguishing peralkaline zircon from zircon from other types of granitoids. Finally, chemical discrimination criteria will be proposed for zircon populations of different provenance.

## 2. Geology of the Studied Plutons and Samples

The geochemical classification of peralkaline granitoids and syenitoids is still rather controversial and we do not intend to engage in this direction. To avoid any possible misunderstanding, however, it should be noted that the term “peralkaline” is used in line with the original definition of Shand [41], i.e., for rocks with  $Al < Na + K$  (molar) (Figure 1a). When necessary, we use the term “A-type granites” for subaluminous to very mildly peraluminous, i.e., “not peralkaline” ( $A > Na + K$ ), granites generally meeting the original definition of A-type rocks by Loiselle and Wones [42]. If samples from a particular suite partially exceed field boundaries, we classified the whole suite according to the majority of samples. This is probably not an ideal solution, but it will help us to briefly define the affiliation of each magmatic rock to a certain geochemical type in the text below.

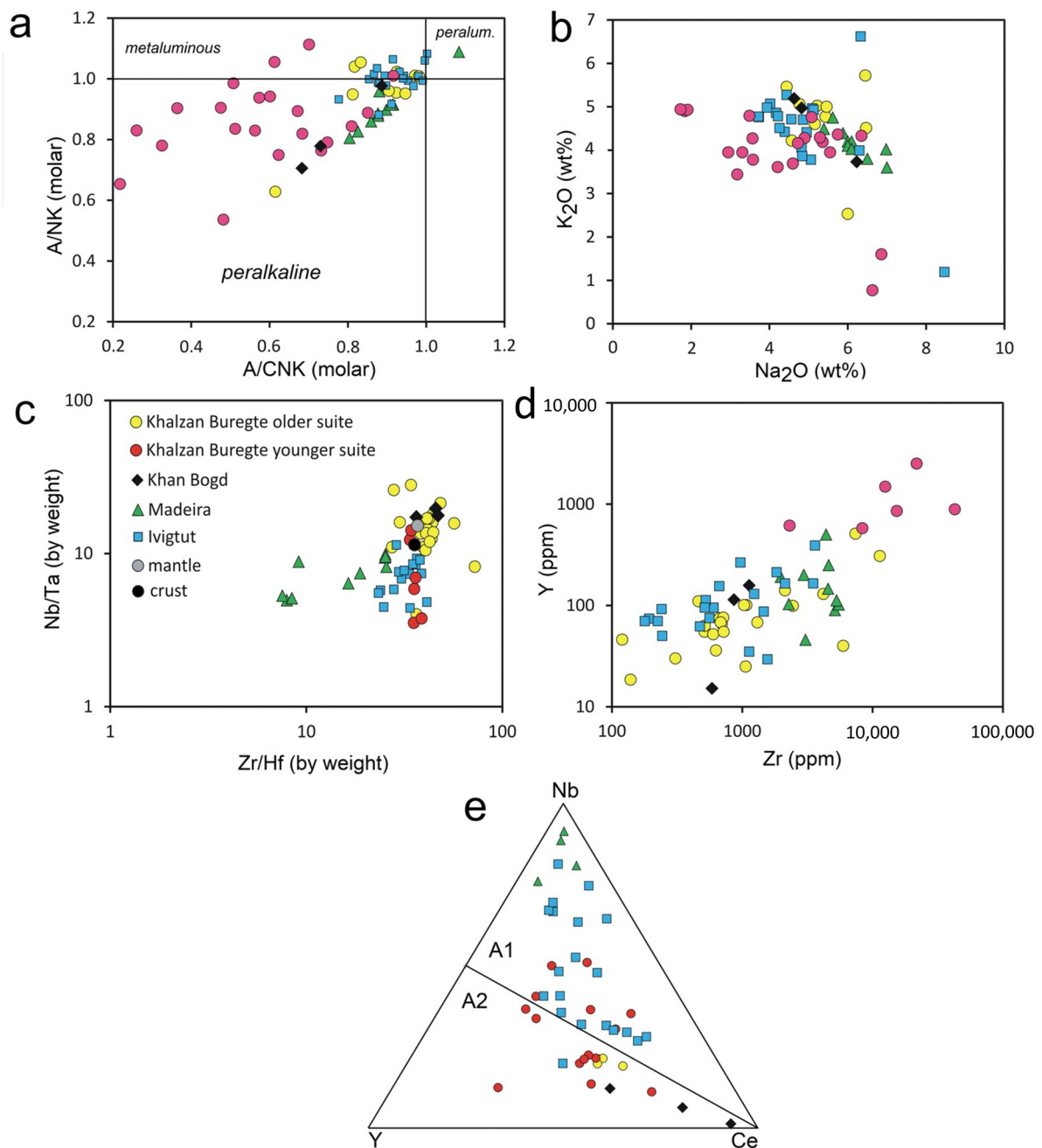


**Figure 1.** Bulk-rock composition of studied peralkaline rocks: (a) classification of peralkaline/peraluminous rock A/CNK vs. A/NK according to Shand [37]; (b) Na<sub>2</sub>O vs. K<sub>2</sub>O; (c) internal fractionation of studied plutons in terms of Zr/Hf vs. Nb/Ta including Earth crust and mantle averages [43,44]; (d) contents of Zr vs. Y; (e) classification of A-type rocks according to Eby [45]. Data are from [32,34,46–49].

Four plutons of peralkaline granitoids with different geological histories and geochemical signatures were selected for this study. The Khan Bogh and Khalzan Buregte plutons, both in Mongolia, represent typical mantle-derived and rift-related [46], F-poor, strongly peralkaline pyroxene-bearing plutons: the Khan Bogh forms a large, rather monotonous, ring-shaped body complemented with a lithologically varied roof zone rich in mineralogically varied dikes; the Khalzan Buregte, a much smaller pluton, is composed of numerous subintrusions of basic to acid lithologies. The Madeira pluton, Brazil, and Ivigtut stock, Greenland, represent mildly peralkaline, dominantly core-derived [47,48] granitic systems

rich in fluorine. The high degree of F saturation and the strong peralkalinity at the end of crystallization resulted in the formation of large, nearly monomineralic bodies of cryolite.

The Khan Bogd pluton, one of the world's largest complexes of peralkaline granites (1500 km<sup>2</sup>), Lower Permian in age, is located in southern Mongolia. It is a part of the Gobi-Tien Shan belt of alkaline rocks related to Late Paleozoic rifting [50]. The well-exposed pluton is composed of two main bodies. The western body is formed by coarse-grained, near-contact porphyritic, aegirine-arfvedsonite granite with common zirconosilicates; its circular structure (ca. 30 km in diameter) is underscored by numerous ring dikes of layered pegmatites and aegerine aplites (ekerites). The smaller (ca. 15 × 13 km) and geologically younger eastern body is formed by fine-grained aegirine granite. Zircon from three samples of the main intrusive phase and three samples of dike rocks were studied.

The Khaldzan Buregte pluton (also Khaldzan Burgedei, ca 100 km<sup>2</sup>), Upper Devonian in age, is located near Chovd town in western Mongolia. Kovalenko et al. [46] distinguished two intrusive suites and divided them into seven intrusive phases. The older suite is composed of voluminous intrusions of nordmarkite (peralkaline quartz-bearing syenite) and peralkaline granite forming a substantial part of the pluton (phases 1 + 2), dikes of peralkaline aplite (locally termed as ekerite, phase 3) and dikes of peralkaline rhyolite (locally termed pantellerite, phase 4). The younger suite is formed by a stock (0.85 km<sup>2</sup>) of peralkaline rare-metal granite (RMG) with pericontact pegmatoidal facies (phase 5) intruded by syenite dikes (phase 6) and by stock (0.05 km<sup>2</sup>) of miarolitic peralkaline rare-metal amazonite granite (RMG, phase 7). Besides quartz and alkali feldspars, the RMGs contain common fluorite, Na-amphiboles, and zircon. Indications of Nb mineralization were found in granitoids of the older intrusive suite [36].

Zircon from altogether 11 samples from phases 2, 3, 4, 5, and 7 was studied.

The Ivigtut granite stock with the associated famous cryolite deposit is located at the sea coast in southwestern Greenland as a member of the Gardar alkaline igneous province [51]. Granite forms a cylindrical body 300 m across (ca 0.1 km<sup>2</sup>), intruding Archean gneiss and surrounded by a thin zone of intrusive breccia. The slightly peralkaline-subaluminous granite ( $A/NK = 0.98\text{--}1.08$ ) shows vertical zoning changing from a hypersolvus texture on the surface to subsolvus texture below the former cryolite deposit at the depth of 300–700 m. Different degrees of alteration (albitization, greisenization, sericitization) were detected in the whole known vertical section [48,51]. The source of F, Na, and CO<sub>2</sub>-rich metasomatizing fluid/melt (?) was interpreted in the lithospheric mantle enriched via subduction during the Ketilidian orogeny [52]. The relatively fresh granite domains are composed of quartz, alkali feldspars with minor edenitic amphibole and biotite and accessory cryolite, zircon, fluorite, and siderite. Bodies of simple pegmatite were found near the upper border of the cryolite body, while granophyre dikes and zircon-rich quartz-K-feldspar dikes cut the gneiss close to the granite stock. The cryolite body is inhomogeneous, containing domains rich in quartz, siderite, topaz, or fluorite [51]. Four samples were analyzed, representing granite, pegmatite, dike rocks, metasomatite, and the cryolite body.

The Madeira pluton (1824–1818 Ma, 60 km<sup>2</sup>) [47] is situated in the central part of the Amazon Craton, Brazil. It consists of four principal rock types [53,54]. The early porphyritic amphibole-biotite “rapakivi” granite was followed by biotite granite. Both granites were later intruded by a sheet-shaped body of hypersolvus granite and peralkaline cryolite-bearing albite granite. The latter contains two major zones of thick veins and pods of cryolite and a number of nests of intragranitic cryolite-rich pegmatites [49]. Albite granite is strongly but inhomogeneously enriched in F (max. more than 3 wt%), Rb (max. 0.7 wt%), Zr (~0.7 wt%), Sn (~0.2 wt%), Nb, Th, Pb, Hf, Y, REE, etc. [47,53]. Four samples from core peralkaline granite and cryolite pegmatite pods have been already analyzed [16] and are shown here for comparison.

In order to reflect the widest variety of chemical compositions of zircon from peralkaline granitoids, published zircon data from the REE-Nb-Zr-enriched alkaline plutons of Thor Lake and Strange Lake (both Canada) [33,35] and from the Sn, Nb-enriched Al-

Sibai stock (Egypt) [55] are shown for comparison in the diagrams. With the intention of placing the studied zircon samples in the broadest possible context, chemical compositions of zircon from typical strongly peraluminous S-type and sub- to mildly peraluminous A-type granites are also shown in some diagrams for comparison. S-type granites are mainly represented by Variscan occurrences in the Bohemian Massif (Czech Republic and Austria), France, Portugal, and Cornwall [23,56–59], while A-type granites are represented by data from the eastern Erzgebirge (Czech Republic, Germany), Finland, Brazil, and Transbaikalia [16,60].

Important bulk-rock chemical features of the discussed plutons are visualized in Figure 1.

### 3. Methods

Images of zircon in back-scattered electron (BSE) mode and zircon semi quantitative elemental spectra were acquired using TESCAN Vega 3XMU scanning electron microscope (SEM) (TESCAN ORSAY HOLDING, Brno, Czech Republic) equipped with a secondary electron detector (SE), a back-scattered electron detector (BSE) and a micro-analytical system for energy dispersive analysis (EDS) Oxford Instruments Ultim Max 65 with SDD (silicon drift detector) (Oxford Instruments, Abingdon, UK). An accelerating voltage of 20 kV was applied for the acquisitions of microphotographs and also for analytical acquisitions. The absorbed current for acquisitions of microphotographs was set to optimal values to obtain images of the best possible quality at higher magnifications. For the determinations of chemical composition with EDS, the absorbed current was set to achieve the optimum gain/yield of the detector.

Major elements and some minor elements in zircon were analyzed using the Jeol JXA—8230 electron microprobe housed (JEOL Ltd., Akishima, Tokyo, Japan) at the Institute of Geology of the Czech Academy of Sciences, Praha, operated in the wavelength-dispersive mode. Elemental abundances of F, Al, Si, P, S, Ca, Sc, Ti, Mn, Fe, As, Y, Zr, Nb, La, Ce, Nd, Sm, Dy, Er, Yb, Hf, W, Pb, Bi, U, and Th in zircon were determined at an accelerating voltage of 15 kV and a beam current of 15 nA and with a beam diameter ranging from 1 to 2 microns. The counting times on each peak were optimized for individual elements according to their expected concentrations (20–60 s), and twice, half that time was used to obtain background counts on both sides of the peak. Again, X-ray lines and background offsets were selected to minimize interference. The following reference materials were used: fluorite (F), corundum (Al), quartz (Si), apatite (P), barite (S), diopside (Ca), metallic Sc (Sc), rutile (Ti),  $Mn_3O_4$  (Mn), hematite (Fe), gallium arsenide (As), synthetic cubic zirconia (Y, Zr), metallic Nb (Nb), REE glass standard La, Ce, Dy, Er, Nd, Sm, Yb, metallic hafnium (Hf), metallic W (W), crocoite (Pb), metallic Bi (Bi), metallic Th (Th), and metallic U (U). In all minerals, raw data were processed using the PRZ correction procedure (XPP method metal/oxide was applied). Empirically determined correction factors were applied to the overlapping X-ray lines. Detection limits (3 sigma) in wt% are as follows: 0.009 (S), 0.012 (P), 0.013 (Ti), 0.015 (Hf), 0.018 (Ca), 0.020 (Nb, Sc), 0.025 (Si), 0.025 (La, U), 0.027 (Pb), 0.028 (F, Ce), 0.035 (Th), 0.040 (As, Ba), 0.048 (Gd, Mn), 0.050 (Er), 0.060 (Al, Fe, Y), 0.065 (Yb), 0.070 (Na), 0.075 (Zr), and 0.110 (Dy).

Empirical formulae were calculated on the basis of four atoms of oxygen in a formula unit (apfu).

Abbreviations of mineral names in text and figures follow [61]: Amp = amphibole, Cctp = calciocatapleite, Clb = columbite, Crl = cryolite, Flr = fluorite, Gal = galena, Kfs = K-feldspar, Mca = mica, Pl = plagioclase, Px = pyroxene, Qtz = quartz, Thr = thorite, Xnt = xenotime, Zrn = zircon. Other abbreviations used are as follows: NaZr-silik = unknown NaZr silicate, Fe-carb = Fe-dominated carbonate, Fe-ox = iron oxide/hydroxide, SrTh-carb = SrTh-dominated carbonate.

For the list of all studied samples, see Table S1, and for Zr/Hf, Nb/Ta, and Y/Yb values in basic reservoirs, see Table S2 as electronic Supplementary Materials.

## 4. Results

### 4.1. Shape of Zircon Crystals and Aggregates

Zircon in granitoids usually occurs in the form of euhedral crystals with different internal textures that inform about the origin and history of the given crystal. This type of zircon is often described and interpreted in detail, especially in connection with geochronological studies [62]. Non-well textured, often patchy-zoned or vacuolized zircon is studied especially in terms of radioactive damage caused by the presence of U and Th [20,63]. In contrast, anhedral zircon grains and radial, rounded or botryoidal zircon aggregates, poor in, or free of, radioactive elements are much less studied [21]. These very unusual textures of zircon are often found in peralkaline granitoids. Textures of zircon crystals from the four studied plutons, some very unusual, are described in the text below. Especially, the appearance of zircon from the Khan Bogd and Khalzan Buregte plutons is surprisingly variable from sample to sample. This fact cannot guarantee the completeness of the herein-presented overview, despite our best efforts. However, this overview sufficiently illustrates the variability of zircon in peralkaline granitoids.

Euhedral zircon crystals are missing in all studied plutonic rocks as well as in dike rocks of the Khan Bogd pluton. The only possibly primary magmatic zircon was found in Na-pyroxene granite in the form of small isometric rounded crystals, less than 20  $\mu\text{m}$  across, with thin, Hf-enriched rims (Figure 2c). All other zircon varieties are clearly secondary, originated in hydrothermal stage from completely decomposed zirconosilicates (elpidite, armstrongite, gittinsite, calciocatapleite, compare [32]). Rounded aggregates resembling admixtures from a solid solution (zircon in hematitized titanomagnetite or in hydrated Fe oxide, Figure 2a,b) and more common botryoidal aggregates within altered silicates (Figure 2e) were found in aegirine granite of the Khan Bogd main body, while larger rounded grains with sun-resembling corona (Figure 2d), are present in aegirine granite (ekerite) dikes. Very late zircon forming thin veinlets following cleavage of carbonates and crossing crystals of calciocatapleite was found in an aegirine granite dike with local pegmatitic texture (Figure 2f).

At Khalzan Buregte, a principal difference in the shape of zircon crystals was found between the older and the younger intrusive suites, i.e., between phases 1–5 and phase 7 as defined by [46]. In the older suite, relicts of large crystals of primary zirconosilicates (particularly elpidite) decomposed to a mixture of carbonates, aluminosilicates, and irregular zircon aggregates (Figure 3a) together with radially arranged aggregates (Figure 3b) were found in altered granitoids of the main intrusive phase. Nevertheless, small zircon crystals disseminated in fine-grained amphibole matrix among plagioclase crystals (Figure 3c) and somewhat larger well-zoned crystals rich in xenotime component (Figure 3d) indicate that small amounts of zircon may have been primarily in equilibrium with zirconosilicates. In any case, the most common zircon type is represented by rounded or irregular aggregates up to mm in size, with numerous cavities with botryoidal surface (Figure 3e,f), i.e., clearly a secondary and probably low-temperature product of zirconosilicate dissolution and precipitation. Another morphological variety of zircon, enriched in Y and REE, intimately alternates with xenotime, forming lenticular aggregates (Figure 3g).

The younger Khalzan Buregte suite, in contrast, contains exclusively euhedral and zoned zircon crystals, often with metamictized and vacuolized U, Th-rich cores and Hf-enriched well-crystallized rims (Figure 3h–j). Volume changes during the metamictization led to cracking of the rims and their healing with Hf-poor veinlets (Figure 3i).

At Ivigtut, zircon populations from granites and metasomatites dominantly show euhedral crystals although often with enclaves of other minerals (silicates, fluorite, thorite, Figure 4a,b). The crystals are homogeneous in BSE, although some from crystals from the metasomatites are mildly zoned in CL (Figure 4c,d). The only altered, vacuolized, and patchy-zoned zircon was found in carbonatite-induced metasomatite (Figure 4e). An unusual texture of euhedral zircon was found in a quartz–orthoclase vein with a unidirectional solidification texture (UST): here, zircon forms several UST zones overgrowing K-feldspar crystals (Figure 4f). Zircon from granite, pegmatite, and UST-textured dike (Figure 4a,b,f)

is classified, beyond any doubt, as magmatic, while zircon from F-rich metasomatites probably crystallized from high-temperature fluid exsolved from melt during final stage of its evolution. This zircon therefore belongs to the transitional magmatic/hydrothermal stage.

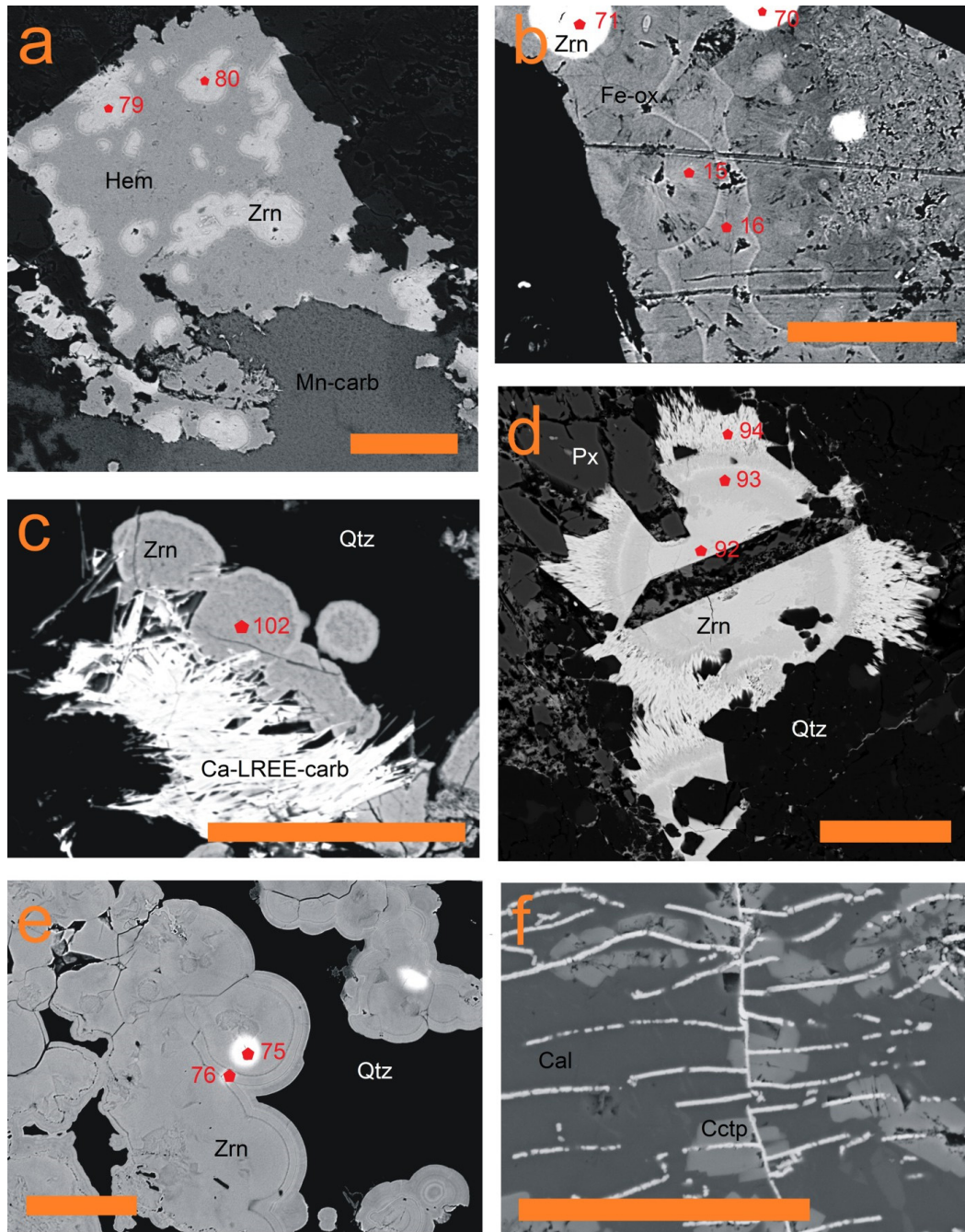


**Figure 2.** BSE-images of zircon and associated minerals from Khan Bogt pluton: (a) grain of hematized titanomagnetite with rounded admixtures of zircon (#KB-2); (b) detail of another hematite grain with maximalized contrast shows radial texture of secondary hematite and domains with different contents of Ti and Zr (#KB-4); (c) rounded grains of zircon with thin Hf-enriched rims partially replaced by Ca-REE carbonate of bastnasite type (#EDG-09); (d) rounded sun-like zircon grain with massive ring-zoned core and corona-shaped rim (#KB-13); (e) botryoidal aggregate of zircon (#KB-4); (f) veinlets of zircon rich in Xnt-component (light) penetrating calcite (dark gray) with crystals of calcic catapleite (medium gray) (#KB-6). The numbers in the figures refer to the analysis numbers in Table 1. Scale bars are 50  $\mu\text{m}$  in all cases.

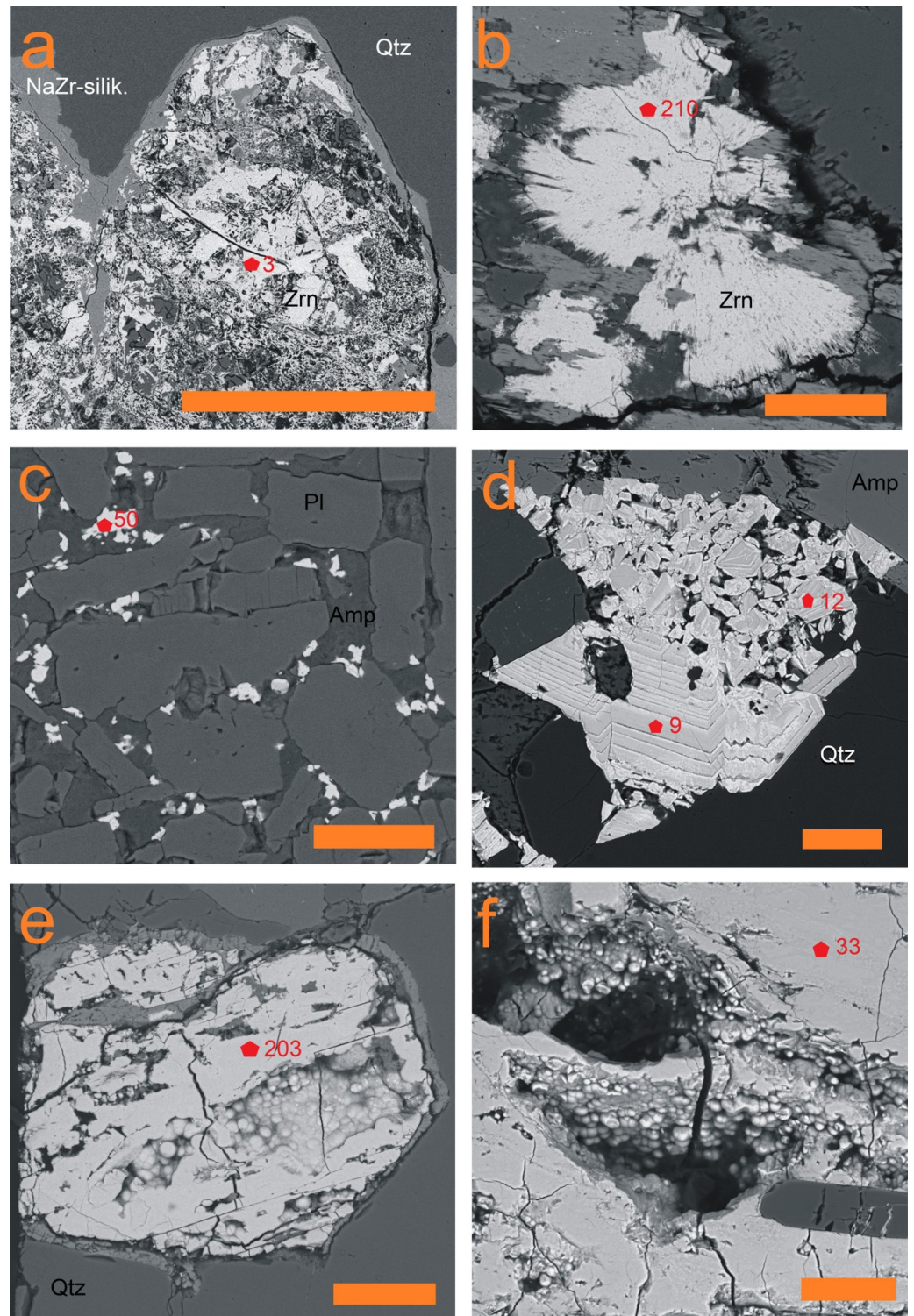
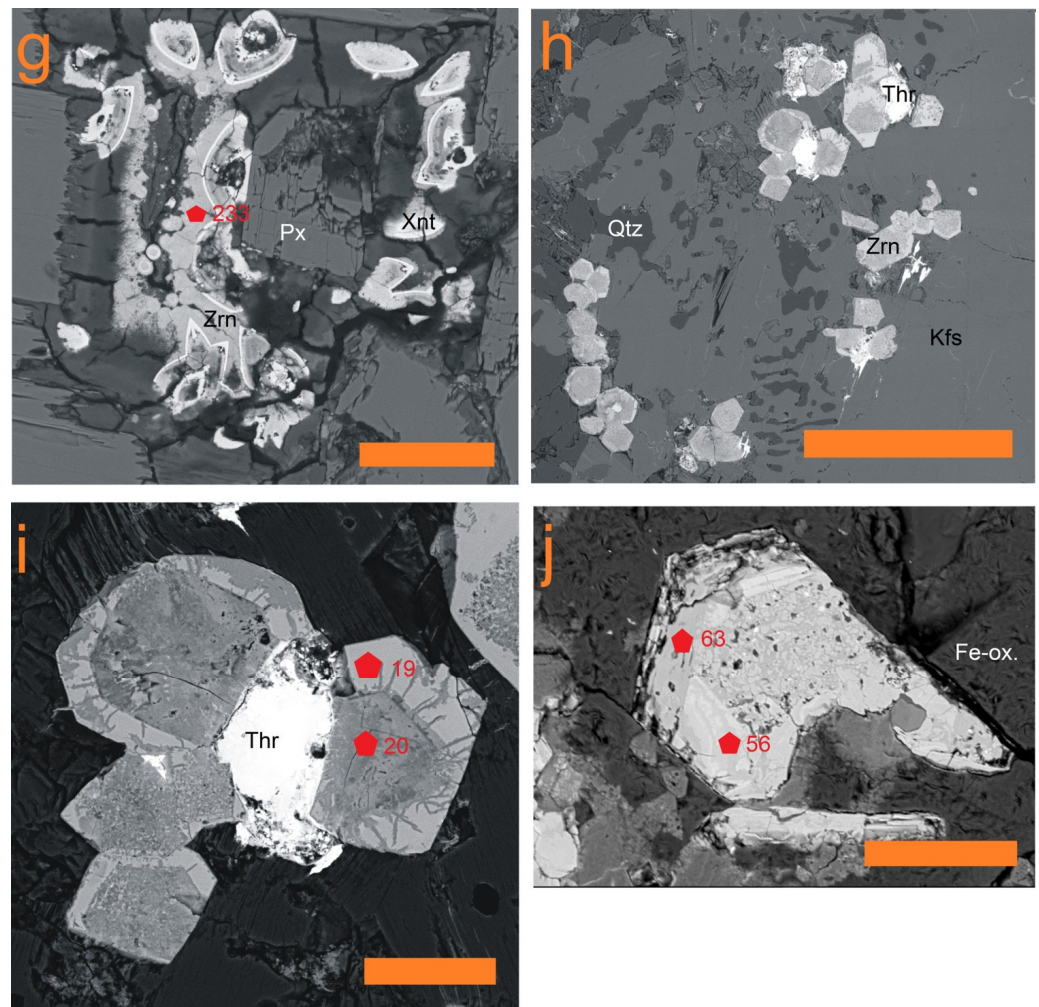


Figure 3. Cont.



**Figure 3.** BSE-images of zircon and associated minerals from Khalzan Buregte pluton: (a) crystal of an unknown primary zirconosilicate fully replaced by aggregate of zircon and mixture of Al, Fe-silicates and Fe, Ca-carbonates. Thin rim of the former crystal is formed with an insufficiently determined Na, Zr-silicate (elpidite?) (KBur-4); (b) radial aggregate of late zircon (#KBur-2); (c) small crystals of zircon in amphibole matrix among albite crystals (#KBur-1); (d) zonal zircon crystals, thin dark zones are enriched in Xnt-component (too thin to be analyzed, #KBur-3); (e) secondary zircon with cavities (#KBur-3); (f) detail of botryoidal surface of cavities within secondary zircon aggregates (#KBur-6); (g) a Zr-Ce-Y phase (light gray)-xenotime (white) lenticular aggregates in altered Na-pyroxene (dark) (#KBur-2); (h) group of strongly zonal zircon crystals in a perthite phenocryst, (#KBur-10); (i) detail of previous picture: U, Th-rich cores are rimmed with Hf-rich rims. Cores are inhomogeneous, metamictized. Changes in core volume during metamictization caused cracking of the rims. White grain is thorite (KBur-10); (j) zircon crystal with metamictized vacuolized core and Hf-enriched rim, #KBur-11). The numbers in the figures refer to the analysis numbers in Table 2. Scale bar is 400  $\mu\text{m}$  in images (a,h) and 50  $\mu\text{m}$  in other cases.

The most monotonous shape of zircon crystals was found at Madeira (Figure 5). The crystals are usually composed of large cores with numerous  $\mu\text{m}$ -sized inclusions of hematite (Figure 5a), thorite (Figure 5d), and different silicates (Figure 5c), and thin rims, somewhat lighter in BSE due to Hf enrichment. Vacuolized cores and patchy zoning were found scarcely (Figure 5e,f) as well as inclusions of zircon and thorite within sulfides (Figure 5b). This zircon should be classified as primary magmatic.

**Table 1.** Chemical composition of typical zircon and associated hematite from Khan Bogd (wt%).

Zircon Type	Zircon in Hematite				Globular Zircon			Sun-like Zircon			Hematite	
	Sample	KB-2	KB-2	KB-4	KB-4	KB-4	KB-4	EDG-09	Core	Rim	Corona	KB-4
Spot	79	80	70	71	75	76	102	92	93	94	15	16
Zr/Hf atomic	90.03	86.63	92.15	126.55	83.16	82.32	98.43	91.06	110.13	93.59		
Y/Yb atomic	22.92	35.35	32.75	21.16	29.08	38.02	16.13	16.72	13.06	18.73		
P <sub>2</sub> O <sub>5</sub>	0.25	0.21	0.25	0.36	0.15	0.07	0.39	0.87	1.51	0.45		
As <sub>2</sub> O <sub>5</sub>	bdl	0.05	0.07	0.13	bdl	0.06	bdl	bdl	bdl	bdl		
Nb <sub>2</sub> O <sub>5</sub>	0.58	0.48	0.43	0.20	0.00	0.06	0.53	0.06	bdl	bdl		
SiO <sub>2</sub>	26.03	27.15	26.84	26.40	27.50	30.47	24.86	29.14	26.03	30.17	2.75	2.40
TiO <sub>2</sub>	0.35	0.34	0.44	0.30	0.22	0.48	0.22	0.12	0.04	bdl	4.01	2.40
ZrO <sub>2</sub>	44.58	47.79	45.63	49.27	49.51	56.86	46.41	53.15	51.94	56.02	0.107	0.071
HfO <sub>2</sub>	0.85	0.94	0.85	0.67	1.02	1.18	0.81	1.00	0.81	1.02	bdl	0.031
ThO <sub>2</sub>	0.36	0.74	0.41	0.94	0.28	0.04	1.16	0.20	0.55	0.47		
UO <sub>2</sub>	0.29	0.21	0.18	0.49	0.25	0.24	0.30	0.24	0.22	0.09		
Y <sub>2</sub> O <sub>3</sub>	6.44	5.03	4.66	7.54	1.63	0.85	5.18	4.36	5.61	6.07	bdl	bdl
Gd <sub>2</sub> O <sub>3</sub>	0.48	0.67	1.67	0.69	0.09	0.13	0.72	0.28	0.42	0.35		
Dy <sub>2</sub> O <sub>3</sub>	0.75	0.45	0.98	0.98	bdl	bdl	0.92	0.57	0.95	1.00		
Er <sub>2</sub> O <sub>3</sub>	0.26	bdl	0.14	0.54	0.10	bdl	0.56	0.29	0.55	0.70		
Yb <sub>2</sub> O <sub>3</sub>	0.49	0.25	0.25	0.62	0.10	bdl	0.56	0.45	0.75	0.57		
Al <sub>2</sub> O <sub>3</sub>	0.78	0.91	1.06	0.59	0.27	0.71	0.75	0.42	0.65	0.06	0.79	1.20
Sc <sub>2</sub> O <sub>3</sub>	bdl	bdl	bdl	bdl	bdl	bdl	bdl	bdl	0.05	bdl		
MnO	0.59	0.33	0.17	0.07	0.24	0.42	0.06	0.16	bdl	bdl	0.16	0.13
FeO *	5.97	5.46	3.77	3.67	1.39	1.60	0.67	2.94	2.21	0.62	91.07	90.51
CaO	0.77	1.00	0.65	1.77	0.97	0.89	2.18	0.39	1.08	0.14		
PbO	0.39	0.17	0.07	0.21	0.04	0.14	0.17	0.03	0.07	0.06		
SO <sub>3</sub>	0.01	0.01	0.02	0.02	0.02	bdl	0.06	0.02	0.02	bdl		
F	bdl	bdl	0.01	0.30	bdl	bdl	0.19	bdl	bdl	bdl		
Total	90.32	92.24	88.54	95.75	83.88	94.35	86.70	94.76	93.47	97.82	98.90	97.66

\* Fe<sub>2</sub>O<sub>3</sub> in hematite; free space—not analyzed; bdl—below detection limit.

**Table 2.** Chemical composition of typical zircon from Khalzan Buregte (wt%).

Phase	Zircon											Ce-Rich Zircon
	2	2	2	3	3	3	3	7	7	7	7	2
Sample	KBur-2	KBur-3	KBur-4	KBur-6	KBur-7	KBur-8	KBur-8	KBur-10	KBur-10	KBur-11	KBur-11	KBur-2
Spot	210	203	3	33	50	9	12	19	22	56	63	233
Zr/Hf atomic	86.92	79.79	84.72	73.35	82.67	68.20	85.48	17.54	25.88	6.78	15.90	166.57
Y/Yb atomic	14.37	27.64		38.31	16.10	14.30	7.51	1.43	2.58	2.61	3.64	15.85
P <sub>2</sub> O <sub>5</sub>	0.81	1.65	0.06	0.29	0.72	3.28	0.44	0.26	0.28	0.19	1.09	3.46
As <sub>2</sub> O <sub>5</sub>	0.02	0.00	bdl	bdl	bdl	bdl	bdl	0.01	0.20	bdl	bdl	1.56
Nb <sub>2</sub> O <sub>5</sub>	0.22	bdl	bdl	bdl	0.29	1.05	bdl	bdl	bdl	0.02	0.17	0.39
SiO <sub>2</sub>	24.37	24.73	29.30	22.03	28.92	22.08	30.94	30.86	24.96	27.99	22.47	24.40
TiO <sub>2</sub>	0.20	0.12	0.26	0.22	0.22	0.29	bdl	bdl	bdl	bdl	0.03	bdl
ZrO <sub>2</sub>	44.19	48.64	59.51	49.08	56.86	47.91	65.05	57.40	48.94	50.67	49.98	17.98
HfO <sub>2</sub>	0.87	1.04	1.20	1.14	1.18	1.20	1.30	5.59	3.23	12.76	5.37	0.18
ThO <sub>2</sub>	bdl	0.03	bdl	bdl	0.03	0.65	0.04	0.37	4.22	1.06	2.92	0.50
UO <sub>2</sub>	0.12	0.04	0.03	0.03	0.11	0.29	0.24	2.54	1.20	0.47	1.75	0.07
Y <sub>2</sub> O <sub>3</sub>	9.20	3.67	0.25	2.27	2.07	6.38	0.50	0.69	1.26	0.86	3.55	10.63
La <sub>2</sub> O <sub>3</sub>	bdl	bdl										0.00
Ce <sub>2</sub> O <sub>3</sub>	0.04	0.21										18.86
Nd <sub>2</sub> O <sub>3</sub>	0.22	0.90										0.43
Gd <sub>2</sub> O <sub>3</sub>	0.46	0.44	bdl	0.41	0.12	0.21	bdl	bdl	0.12	0.08	0.19	0.94
Dy <sub>2</sub> O <sub>3</sub>	1.21	0.67	0.01	0.42	0.38	0.93	0.28	bdl	0.20	0.10	0.56	2.03
Er <sub>2</sub> O <sub>3</sub>	1.16	0.26	bdl	0.11	0.17	0.92	bdl	0.17	0.30	0.12	0.61	1.38
Yb <sub>2</sub> O <sub>3</sub>	1.12	0.23	bdl	0.10	0.22	0.78	0.12	0.84	0.85	0.58	1.70	1.17
Al <sub>2</sub> O <sub>3</sub>	1.80	1.69	1.32	1.05	1.52	0.59	0.06	bdl	1.35	0.51	1.35	2.05
Sc <sub>2</sub> O <sub>3</sub>	bdl	0.05	0.04	bdl	bdl	bdl						
MnO	0.04	0.09	0.33	0.18	0.05	0.08	bdl	bdl	bdl	0.14	0.22	0.13
FeO	0.53	0.37	1.14	0.34	0.64	0.51	0.21	0.23	0.93	0.92	1.60	1.24
CaO	2.36	3.19	0.63	3.38	1.44	1.12	0.16	bdl	0.54	0.57	0.68	2.51
PbO	bdl	bdl	bdl	bdl	bdl	0.16	bdl	0.03	0.22	0.10	0.26	0.07
SO <sub>3</sub>	0.03	0.02	0.02	0.06	0.03	0.04	bdl	bdl	0.04	bdl	bdl	0.04
F	bdl	bdl	bdl	3.00	bdl	0.06	bdl	bdl	0.39	0.63	2.42	0.36
Total	88.99	87.98	94.05	81.14	95.00	88.53	99.37	99.05	89.29	97.77	96.91	90.40

Note: bdl—below detection limit.

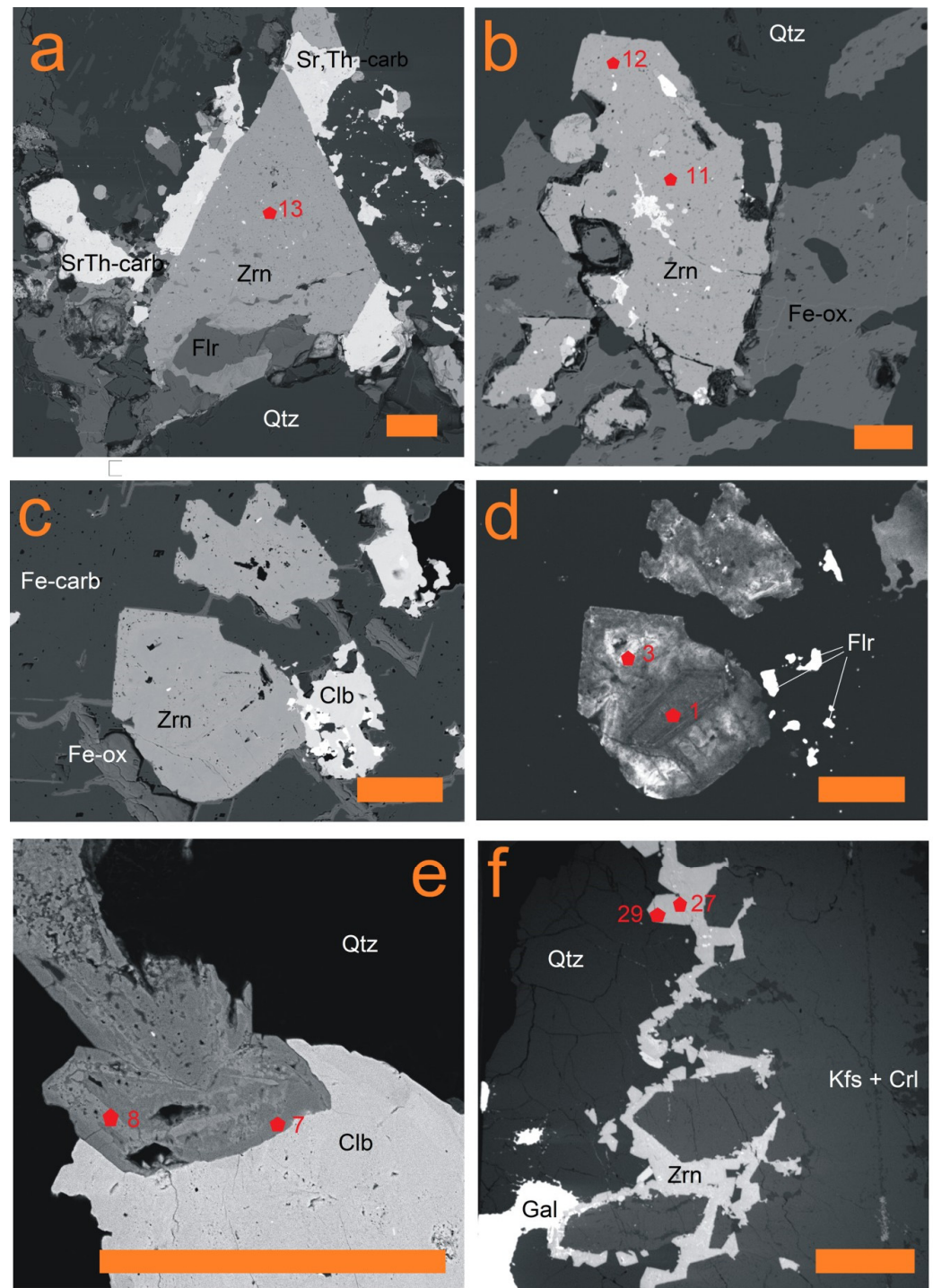


**Figure 4.** BSE-images of zircon and associated minerals from Ivigtut stock: (a) euhedral homogeneous zircon crystal associated with fluorite and Sr, Th-carbonate (granite, #56a); (b) nearly euhedral zircon crystal with inclusions of Sr, Th-carbonate associated with Fe-oxides and quartz (granite, #56a); (c) euhedral zircon crystals associated with columbite with inclusions of Sr, Th, REE-fluoride (light gray and white). Matrix is composed of siderite, along cleavage altered to hydrated Fe-oxide (metasomatite, #34); (d) identical zircon crystals in CL, the white grains being REE-rich fluorite (metasomatite, #34); (e) slightly zoned and vacuolized zircon associated with columbite (carbonatite metasomatite of granite, #X3); (f) unidirectional textures of K-feldspar and quartz completed with zone of oriented crystallization of zircon (Kfs-Qtz vein, #92). The numbers in the figures refer to the analysis numbers in Table 3. Scale bar is 5 mm in image (f) and 100  $\mu$ m in all other images.

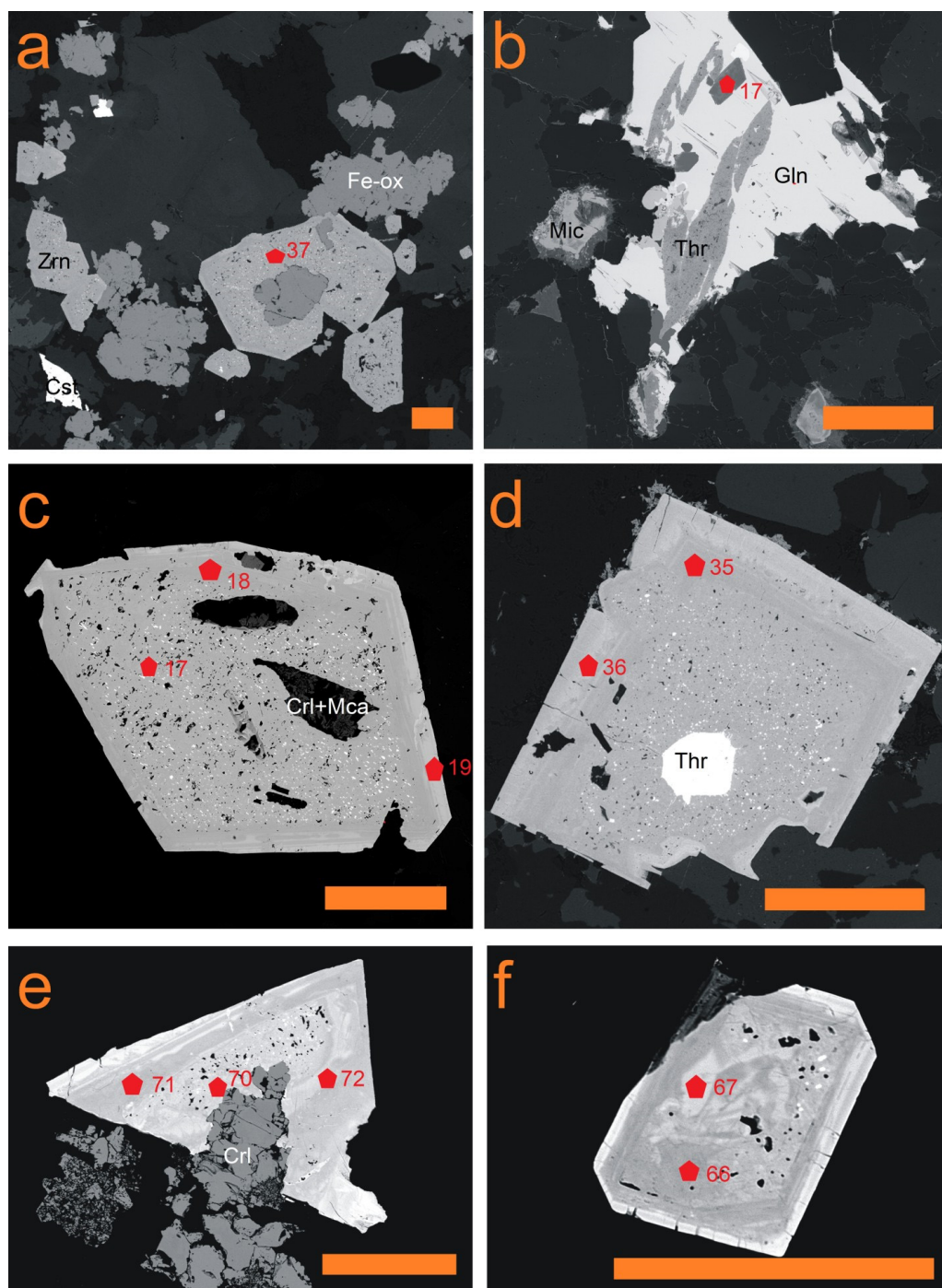


**Figure 5.** BSE-images of zircon and associated minerals from albite-cryolite granite of Madeira pluton: (a) euhedral zircon crystal associated with hematite (#4894); (b) small euhedral zircon crystal in association with thorite, microlite, and galena (#127); (c) vacuolized zircon crystal with cryolite inclusions (dark) (#4894); (d) euhedral zircon crystal with vacuolized core, Hf-enriched rim and thorite inclusion (white) (#4894); (e) zircon crystal with vacuolized core, darker outer zone with lower analytical total, and Hf-rich rim (#4894); (f) euhedral zircon crystal with patchy core and Hf-enriched rim (#4894). The numbers in the figures refer to the analysis numbers in Table 4. Scale bars are 200  $\mu\text{m}$  in all cases.

**Table 3.** Chemical composition of typical zircon from Ivigtut (wt%).

	Metasomatite		Granite			Carbonatite Metasomatite		Kfs-Zrn Vein	
Sample	Iv-34		Iv-56a			Iv-X3		Iv-92	
Spot	1	3	11	12	13	7	8	27	29
Zr/Hf atomic	35.35	32.89	43.67	32.75	39.12	37.36	17.90	49.95	32.68
Y/Yb atomic	3.38	1.22	4.69	1.69	2.74	2.01	2.85	6.86	4.15
P <sub>2</sub> O <sub>5</sub>	0.78	0.78	0.77	0.40	0.59	0.46	0.24	1.54	0.74
As <sub>2</sub> O <sub>5</sub>	bdl	bdl	bdl	bdl	bdl	bdl	bdl	bdl	bdl
Nb <sub>2</sub> O <sub>5</sub>	0.04	bdl	0.13	bdl	bdl	1.80	0.15	0.12	bdl
SiO <sub>2</sub>	31.15	31.03	26.73	31.20	31.24	29.47	29.36	28.16	29.91
TiO <sub>2</sub>	bdl	bdl	bdl	bdl	bdl	0.07	bdl	bdl	bdl
ZrO <sub>2</sub>	62.70	62.96	57.77	63.46	63.44	62.32	59.32	51.75	59.88
HfO <sub>2</sub>	3.03	3.27	2.26	3.31	2.77	2.85	5.66	1.77	3.13
ThO <sub>2</sub>	0.08	0.07	0.20	bdl	0.07	0.18	0.24	3.56	0.22
UO <sub>2</sub>	0.05	bdl	0.90	0.08	bdl	0.14	0.21	0.42	0.14
Y <sub>2</sub> O <sub>3</sub>	0.89	0.49	1.80	0.33	0.55	0.60	0.67	4.13	1.19
Dy <sub>2</sub> O <sub>3</sub>	0.21	0.08	0.38	0.15	0.04	0.24	bdl	0.69	0.11
Er <sub>2</sub> O <sub>3</sub>	0.28	0.19	0.43	0.14	0.21	0.19	0.21	0.83	0.29
Yb <sub>2</sub> O <sub>3</sub>	0.46	0.70	0.67	0.34	0.35	0.52	0.41	1.05	0.50
Al <sub>2</sub> O <sub>3</sub>	bdl	bdl	0.47	0.04	bdl	0.05	0.22	bdl	0.13
Sc <sub>2</sub> O <sub>3</sub>	bdl	bdl	bdl	bdl	bdl	bdl	bdl	bdl	bdl
MnO	bdl	0.03	0.15	0.05	bdl	0.09	bdl	bdl	0.07
FeO	0.11	0.24	2.49	0.22	0.09	0.76	0.27	0.17	1.12
CaO	bdl	0.01	0.21	0.05	bdl	bdl	0.11	0.39	0.05
PbO	0.04	bdl	0.03	bdl	bdl	bdl	0.03	0.13	0.16
SO <sub>3</sub>	bdl	bdl	bdl	bdl	bdl	bdl	bdl	bdl	bdl
F	bdl	bdl	1.44	bdl	bdl	bdl	0.06	3.15	0.08
Total	99.83	99.87	96.85	99.84	99.36	99.75	97.17	97.91	97.74

Note: bdl—below detection limit.

**Table 4.** Chemical composition of typical zircon from Madeira (wt%).

	Cryolite Granite						Cryolite Granite			Cryolite Granite		
Sample	4894						4894A			PHR 127		
Spot	66	67	70	71	72	17	18	19	35	36	37	17
Zr/Hf atomic	31.85	24.96	22.60	30.67	27.21	33.05	35.96	21.00	29.76	20.05	30.79	7.69
Y/Yb atomic	2.60	1.48	1.14	1.61	30.62	2.02	1.61	0.87	0.76	0.55	0.10	0.40
P <sub>2</sub> O <sub>5</sub>	0.25	0.17	0.22	0.27	0.09	0.47	0.13	0.87	0.53	0.76	0.03	0.10
As <sub>2</sub> O <sub>5</sub>	bdl	bdl	bdl	bdl	bdl	bdl	bdl	bdl	bdl	bdl	bdl	bdl
Nb <sub>2</sub> O <sub>5</sub>	0.04	bdl	0.04	0.03	bdl	bdl	0.06	bdl	bdl	bdl	bdl	bdl
SiO <sub>2</sub>	29.26	31.42	31.23	29.68	31.43	30.34	30.69	30.75	30.41	31.29	31.87	31.02
TiO <sub>2</sub>	bdl	bdl	bdl	bdl	bdl	bdl	bdl	bdl	bdl	bdl	bdl	bdl
ZrO <sub>2</sub>	58.73	62.38	61.64	59.25	63.72	61.33	63.57	61.23	59.70	59.61	62.33	56.16
HfO <sub>2</sub>	3.15	4.27	4.66	3.30	4.00	3.17	3.02	4.98	3.43	5.08	3.46	12.48
ThO <sub>2</sub>	0.18	0.11	0.06	0.11	0.04	0.59	bdl	0.04	0.08	0.05	bdl	0.07
UO <sub>2</sub>	0.23	0.06	bdl	0.07	0.04	0.13	0.15	bdl	0.09	bdl	bdl	bdl
Y <sub>2</sub> O <sub>3</sub>	0.59	0.20	0.22	0.43	0.11	0.51	0.12	0.52	0.34	0.43	bdl	bdl
Dy <sub>2</sub> O <sub>3</sub>	bdl	bdl	bdl	bdl	bdl	bdl	bdl	bdl	0.24	0.16	bdl	bdl
Er <sub>2</sub> O <sub>3</sub>	0.12	0.05	0.17	0.16	0.05	bdl	bdl	bdl	0.29	0.47	0.12	0.07
Yb <sub>2</sub> O <sub>3</sub>	0.39	0.24	0.34	0.46	0.01	0.44	0.13	1.04	0.78	1.37	0.18	0.13
Al <sub>2</sub> O <sub>3</sub>	0.24	bdl	bdl	0.29	bdl	0.07	bdl	bdl	bdl	bdl	bdl	bdl
Sc <sub>2</sub> O <sub>3</sub>	bdl	bdl	bdl	bdl	bdl	bdl	bdl	bdl	bdl	bdl	bdl	bdl
Bi <sub>2</sub> O <sub>3</sub>	bdl	bdl	bdl	bdl	bdl	bdl	bdl	bdl	0.11	bdl	0.07	bdl
MnO	0.44	bdl	bdl	0.32	0.07	0.34	0.28	bdl	0.37	bdl	bdl	bdl
FeO	1.32	0.14	bdl	0.78	bdl	0.56	0.58	bdl	0.68	0 bdl	0.07	0.14

Table 4. Cont.

Sample	Cryolite Granite							Cryolite Granite			Cryolite Granite	
	4894							4894A			PHR 127	
CaO	0.06	0.03	bdl	0.05	bdl	bdl	bdl	0.03	bdl	bdl	bdl	bdl
PbO	0.07	bdl	bdl	bdl	bdl	0.06	bdl	0.04	bdl	bdl	bdl	0.07
SO <sub>3</sub>	bdl	bdl	bdl	bdl	bdl	bdl	bdl	bdl	bdl	bdl	bdl	bdl
F	0.46	bdl	bdl	0.22	bdl	bdl	bdl	bdl	0.19	bdl	bdl	bdl
Total	95.62	99.16	98.68	95.53	99.59	98.02	98.79	99.53	97.63	99.70	98.64	100.26

Note: bdl—below detection limit.

#### 4.2. Chemical Composition

About 245 new complex EPMA analyses were performed for the purpose of this study; the most typical of them are listed in Tables 1–4 and localized in Figures 2–5. In Figures 6–8, the new analyses are complemented with our older analyses from Madeira [16] and by 55 published data from peralkaline systems at Thor Lake, Strange Lake, and El-Sibai [33,35,55] and in some diagrams also by ca. 270 data on zircons from A-type granites and 438 data on zircons from S-type granites, all performed by the first author during the past 15 years [16,23,31,56–58,64] for comparison.

Analytical totals for zircon from peralkaline rocks are often significantly lower than the expected 100 wt%. The totals found are slightly reduced (to 96–98 wt%) in some zircon from Madeira and Ivigtut, but often deeply reduced in zircon from Khan Bogd and the older suite of Khalzan Buregte down to 85–90 wt% in the globular form of zircon (Figure 6a). The low-total zircons are often enriched in Ca and Al (see below).

Hafnium is chemically very similar to zirconium, and mineral hafnon (HfSiO<sub>4</sub>) is isostructural to zircon; consequently, Hf is present in all zircon crystals, mostly in the range of 0.5–1 wt% HfO<sub>2</sub>, Figure 6b). The highest contents of Hf among the studied samples were found at Madeira (usually 3–4, occasionally up to 12 wt% HfO<sub>2</sub>), the younger suite of Khalzan Buregte (usually 2–6, occasionally up to 8 wt% HfO<sub>2</sub>), and at Ivigtut (2–3 wt% HfO<sub>2</sub>). At Khan Bogd and the older suite of Khalzan Buregte, Hf amounts reach only 1.0–1.5 wt% HfO<sub>2</sub>, similarly to those in the Thor Lake and Strange Lake mineralized plutons (Figure 6c).

A general rule is that the Hf contents increase, then the Zr/Hf ratios decrease, with a progressive fractionation of the melt [60,65]: the Zr/Hf value serves as a prominent indicator of magma evolution and a suitable base for graphic expression of zircon chemistry (Figure 7).

Yttrium is another common trace to minor element in zircon, while mineral xenotime (YPO<sub>4</sub>) is isostructural with zircon. Its contents reach max. 9–10 wt% Y<sub>2</sub>O<sub>3</sub>. The enrichment in Y is distinctly antagonistic to that in Hf (Figure 6c): the highest Y contents (mostly >2 wt% Y<sub>2</sub>O<sub>3</sub>) were found at Khan Bogd and in the older suite of Khalzan Buregte (similar to Strange Lake and Thor Lake Zr–REE deposits), while zircon from Madeira usually contains less than 1 wt% Y<sub>2</sub>O<sub>3</sub>. Zircon crystals enriched in both Hf and Y have not been found in peralkaline rocks, which is different to the situation in mildly peraluminous A-type granites (Figure 6d).

Zircon is often enriched in HREE, which enter the zircon lattice together with Y as a xenotime molecule. It is therefore not surprising to find a good positive correlation between Gd, Dy, and Er with Y regardless of the pluton studied: Gd<sub>2</sub>O<sub>3</sub> ≈ 0.9 × Y<sub>2</sub>O<sub>3</sub> (Figure 6e), Dy<sub>2</sub>O<sub>3</sub> ≈ 0.18 × Y<sub>2</sub>O<sub>3</sub>, Er<sub>2</sub>O<sub>3</sub> ≈ 0.12 × Y<sub>2</sub>O<sub>3</sub> (all in wt%). The highest contents found reached ca. 0.8 wt% Gd<sub>2</sub>O<sub>3</sub>, 2 wt% Dy<sub>2</sub>O<sub>3</sub>, and 1.4 wt% Er<sub>2</sub>O<sub>3</sub>, all in zircons from the older suite at Khalzan Buregte. Somewhat lower contents were found in zircon from Khan Bogd (0.8 wt%, 1 wt%, and 0.6 wt%, respectively), while the contents of all the mentioned elements at Madeira and Ivigtut do not exceed 0.2 wt%.

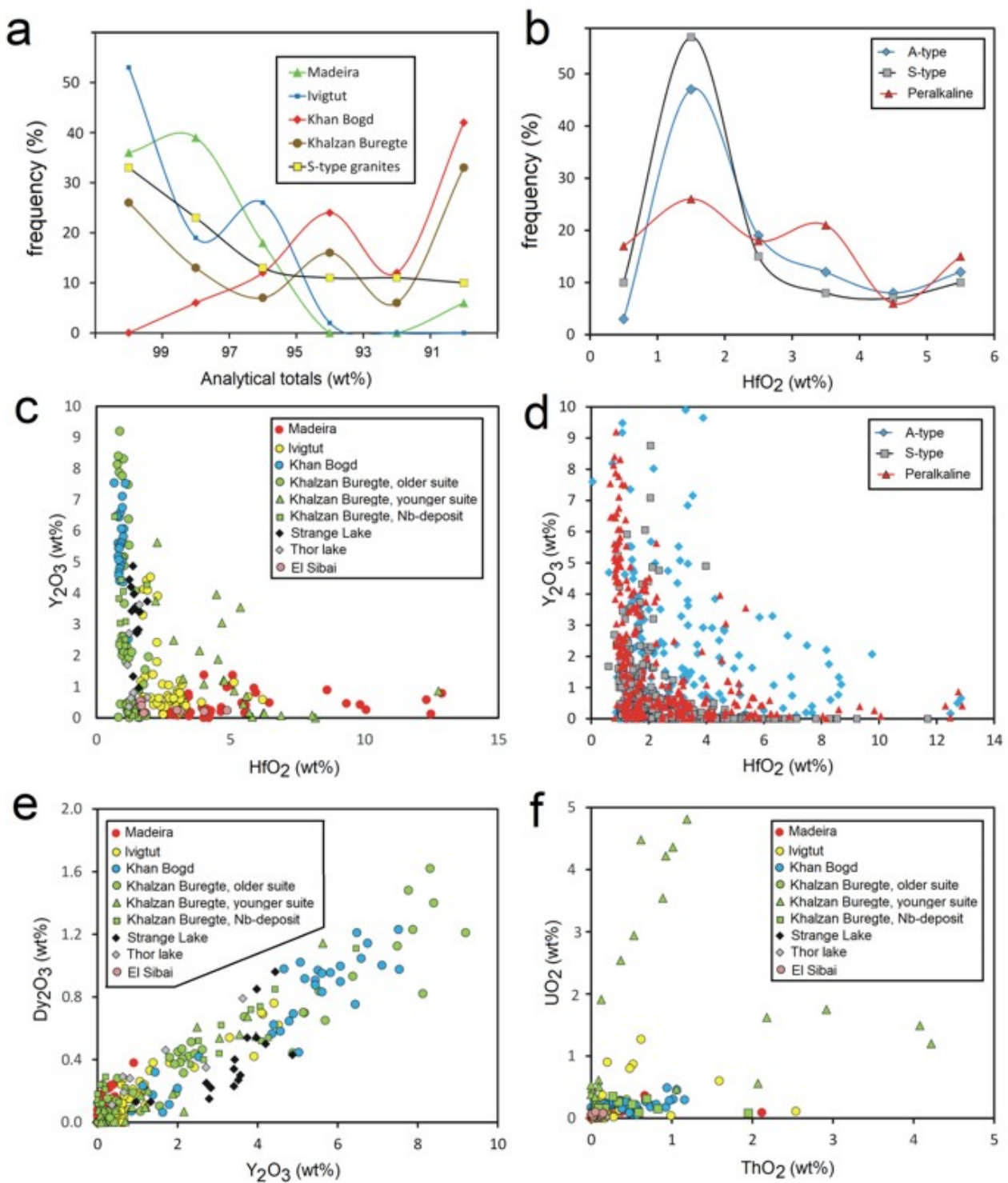


**Figure 6.** Contents of some minor elements in zircon from peralkaline rocks (in wt%) and their comparison with zircon from peraluminous S-type and subaluminous A-type rocks: (a) analytical totals in zircon of zircon from studied peralkaline plutons and common S- and A-type granites; (b) distribution of HfO<sub>2</sub> contents in zircon of different geochemical affiliation; (c) contents of HfO<sub>2</sub> vs. Y<sub>2</sub>O<sub>3</sub> in zircon from peralkaline rocks; (d) contents of HfO<sub>2</sub> vs. Y<sub>2</sub>O<sub>3</sub> in zircon from peralkaline rocks, S-type granites, and A-type granites; (e) contents of Y<sub>2</sub>O<sub>3</sub> vs. Dy<sub>2</sub>O<sub>3</sub> in zircon from peralkaline rocks; (f) contents of ThO<sub>2</sub> vs. UO<sub>2</sub> in zircon from peralkaline rocks. Data from Khalzan Buregte mineralized rocks [36], Thor Lake [33], Strange Lake [35], El-Sibai [55], and author’s data.

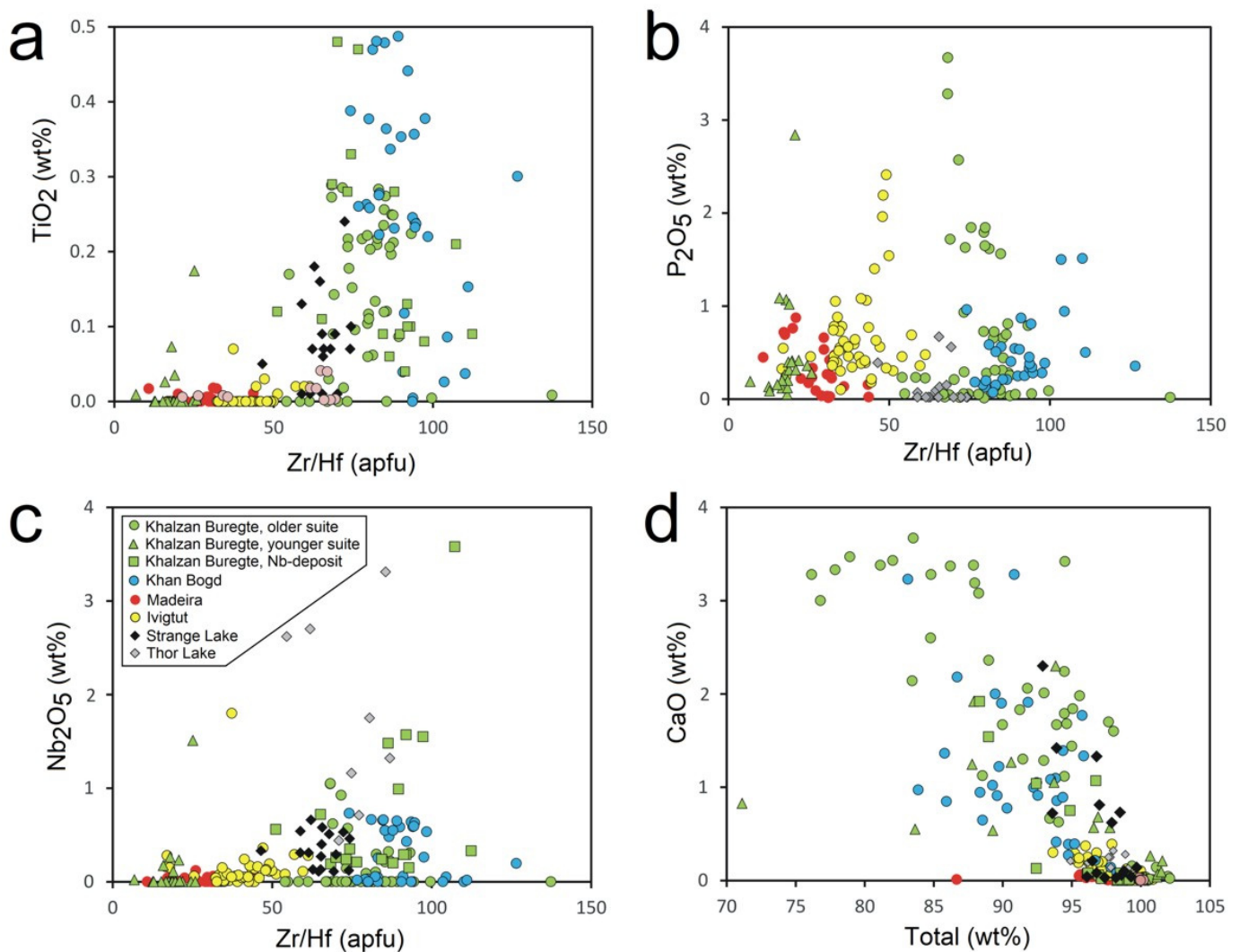


**Figure 7.** Chemical composition of studied zircons from peralkaline rocks in apfu and wt%: (a) Zr/Hf vs. TiO<sub>2</sub>; (b) Zr/Hf vs. P<sub>2</sub>O<sub>5</sub>; (c) Zr/Hf vs. Nb<sub>2</sub>O<sub>5</sub>; (d) analytical total vs. CaO. Data are as in Figure 6.

However, the behavior of Yb contrasts with this, being very different: the ratio of Yb vs. Y differs significantly depending on the rock type (see the Discussion): it increases from ca. 0.1 at Khan Bogd and in the older suite of Khalzan Buregte to over 1 at Madeira. The mineralized domains of Thor Lake [33], Strange Lake [35], and Khalzan Buregte [36] show moderate values. The highest Yb values of max. 2 wt% Yb<sub>2</sub>O<sub>3</sub> were found in the younger suite of Khalzan Buregte, contents lower than 0.6 wt% Yb<sub>2</sub>O<sub>3</sub> at Khan Bogd. The contents of Yb at other sites varied strongly, usually between 0.2 and 1.0 wt% Yb<sub>2</sub>O<sub>3</sub> (see Discussion section for further detail).

Zircon crystals usually show only very small contents of LREE [22]. Nevertheless, we found secondary zircons with 3.2–4.1 wt% Ce<sub>2</sub>O<sub>3</sub> and 0.5–0.75 wt% Nb<sub>2</sub>O<sub>3</sub> (sample 13) and even a transitional phase (ZrYCe)(SiPAs) with 17–20 wt% Ce<sub>2</sub>O<sub>3</sub> (Figure 3g, Table 2, spot 233) in Px-syenite of the older suite at Khalzan Buregte. It is worth mentioning that La is below the EPMA detection limit, indicating an effective separation of Ce and La during the alteration of primary zirconosilicates, probably at highly oxidative conditions.

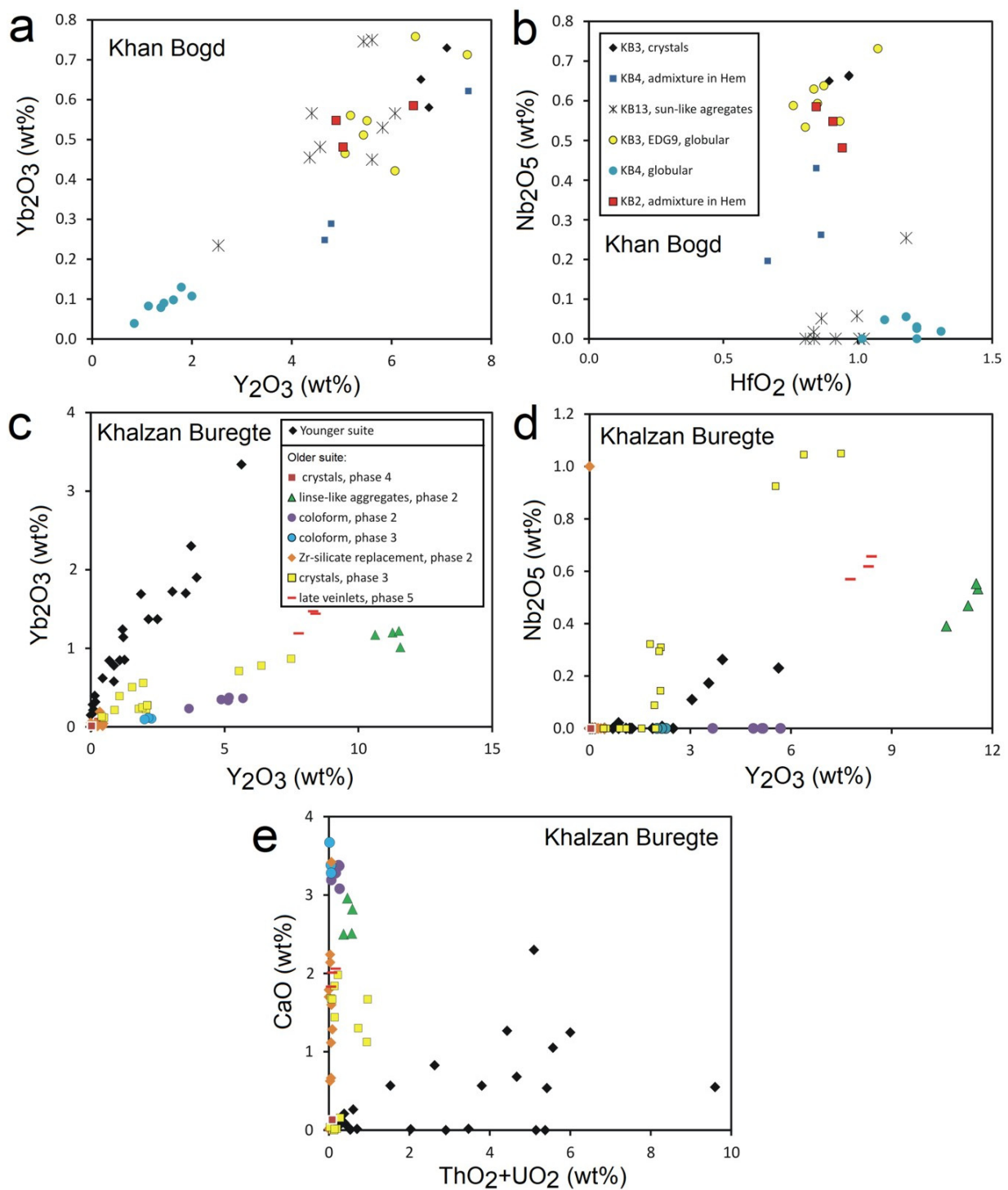


**Figure 8.** Chemical composition of differently shaped zircon from Khan Bogd and Khalzan Buregte plutons: (a) Y<sub>2</sub>O<sub>3</sub> vs. Yb<sub>2</sub>O<sub>3</sub> at Khan Bogd; (b) HfO<sub>2</sub> vs. Nb<sub>2</sub>O<sub>5</sub> at Khan Bogd; (c) Y<sub>2</sub>O<sub>3</sub> vs. Yb<sub>2</sub>O<sub>3</sub> at Khalzan Buregte; (d) Y<sub>2</sub>O<sub>3</sub> vs. Nb<sub>2</sub>O<sub>5</sub> at Khalzan Buregte; (e) (ThO<sub>2</sub> + UO<sub>2</sub>) vs. CaO at Khalzan Buregte; two areas with different type of alteration, i.e., increase in Nb, Ce, and Y vs. decrease in all traces are visible.

The contents of radioactive elements U and Th in zircon crystals from peralkaline granitoids is relatively low, mostly <1 wt% ThO<sub>2</sub> and <0.5 wt% UO<sub>2</sub>. The only exception is the younger suite of Khalzan Buregte with 0.5–4 wt% of the two oxides (Figure 6f).

The contents of titanium usually range between 0.1 and 0.25 wt% TiO<sub>2</sub> in the older suite of Khalzan Buregte, and 0.25–0.45 wt% at Khan Bogd and in mineralized domains of Khalzan Buregte. In other rocks, Ti contents are negligible (Figure 7a).

Phosphorus is a common minor element in zircon entering the crystal lattice along with xenotime substitution; nevertheless, its contents in zircon from the studied peralkaline granitoids usually do not exceed 0.5 wt% P<sub>2</sub>O<sub>5</sub>. Exceptions are some zircons from Khan Bogd and the older suite of Khalzan Buregte, especially those of low totals, reaching 1 and 2.5 wt% P<sub>2</sub>O<sub>5</sub>, respectively (Figure 7b).

The contents of Nb in zircon have been only scarcely analyzed: values of max. 4.5 wt% Nb<sub>2</sub>O<sub>5</sub> were reported from the Cínovec A-type granite, Erzgebirge [16], and values of 6.6 wt% from Thor Lake [37]. In the studied plutons, contents of ca. 0.5 wt% Nb<sub>2</sub>O<sub>5</sub> were often found in zircon from Khan Bogd and scarcely in zircon from Ivigtut and Khalzan Buregte (Figure 7c).

Tantalum was not found in zircon from peralkaline granitoids, although zircon from LCT pegmatite Tanco (Canada) was found to contain up to 2.6 wt% Ta<sub>2</sub>O<sub>5</sub> at Nb below detection limit of EPMA [66].

An enrichment in non-formula elements Al, Ca, Fe, and Mn is typical for low-total (<95 wt%) zircons, whatever is the reason for the structural violation. Elements Al and Ca show a good positive correlation; their highest contents, 0.5–2.0 wt% Al<sub>2</sub>O<sub>3</sub> and 1.5–3.5 wt% CaO, were found in zircons from the older suite at Khalzan Buregte, somewhat lower contents (0.5–1.0 and 0.5–2.0 wt%, respectively) at Khan Bogd. Values exceeding 0.2 wt% of the two element oxides were only uniquely found at Madeira and Ivigtut (Figure 7d). Elements Fe and Mn behave differently, with contents up to 1 wt% FeO and 0.1 wt% MnO being common also in zircons with totals near 100 wt%. Nevertheless, an enrichment of max. 5 wt% FeO was found in low-total zircons from Khan Bogd, and an enrichment of 0.2–0.4 wt% MnO was found in low-total zircons from Khan Bogd and Khalzan Buregte. Rather surprising in this context is the enrichment exclusively in MnO in the range of 0.15–0.45 wt% in zircons with totals of 95–98 wt% from Madeira, which are simultaneously free of Fe, Ca, and Al.

The contents of Sc in zircon from peralkaline granitoids are very low, generally near the EPMA detection limit. Only slightly higher values around 0.04 wt% Sc<sub>2</sub>O<sub>3</sub> were found at Khan Bogd. Low Sc values seem to be a specific feature of peralkaline zircons, while contents 0.1–1 wt% Sc<sub>2</sub>O<sub>3</sub> are typical for zircons from less fractionated S-type granites, and contents up to 2–3 wt% have been reported from zircons from mildly peraluminous A-type granites [16].

Some enrichment in Pb was found in low-totals zircons, with maxima of ca. 0.15 wt% PbO at Khan Bogd, at Khalzan Buregte, and in Kfs-zircon veinlets at Ivigtut, and 0.3 wt% PbO was occasionally found at Madeira in association with galena.

Elevated contents of fluorine of max. 1.5 wt% F, in exclusive grains max. 3 wt% F, were found in zircons with totals of <97 wt% from Ivigtut and scarcely from Khalzan Buregte. Zircon from cryolite granite at Madeira is F-free, although it developed in F-rich environment. Among the published analyses, Thor Lake zircons contain max. 1.7 wt% F [33]. For comparison, fluorine contents of 1–2 wt% in zircons from evolved S- and A-type granites are quite common [16].

Sulphur sometimes enters the zircon structure in the form of an “anhydrite component” (CaSO<sub>4</sub>). Slightly enriched values around 0.05 wt% SO<sub>3</sub> were found in the rocks from Khalzan Buregte and Khan Bogd. Much higher values, up to 0.4 wt%, have been reported from Strange Lake zircons [35]. Even higher values are known from the mildly peraluminous Cínovec A-type granite [16].

## 5. Discussion

### 5.1. General Classification of Studied Peralkaline Plutons and Their Zircon

The studied plutons can be classified into two geochemically distinct groups: (i) strongly peralkaline F-poor Px-bearing granite pluton at Khan Bogd and the older suite of granite +

syenite pluton at Khalzan Buregte; and (ii) and mildly peralkaline F-enriched Px + Mca-bearing granite plutons of Ivigtut and Madeira, and the younger suite of Khalzan Buregte. These two rock groups correspond to two contrasting types of zircon mineralogy:

1. The strongly peralkaline rocks contain only little or no magmatic zircon; the primary carriers of Zr were different zirconosilicates [32,46,50,67]. During post-magmatic hydrothermal stage, zirconosilicates were altered and, almost without residue, replaced with a mixture of zircon with different allumosilicates, carbonates, and Fe-oxides/hydroxides (Figures 2f and 3a). Hydrothermal zircon forms mostly globular or radial aggregates. Both rare primary and common hydrothermal zircons exhibit identical primitive Zr/Hf values;
2. The mildly peralkaline rocks, containing small amounts of Fe-mica along the Napyroxene, exhibit evolved to strongly evolved Zr/Hf, Nb/Ta, and Y/Yb values, are enriched in fluorine, and contain Hf-rich zircon as the exclusive primary Zr mineral. This zircon is almost magmatic-like in all samples from Madeira and granite and pegmatite samples from Ivigtut, but it can also be a product of crystallization of fluids admixed directly from the magma during magmatic/hydrothermal transition, i.e., with a minimum time delay from orthomagmatic zircon, like in metasomatized zones at Ivigtut. (A similar direct transition from peralkaline magma to the hydrothermal stage was described from the Strange Lake pluton [68,69].) Zircon from the magmatic/hydrothermal transition stage is also called “primary” zircon, because it was formed by primary crystallization of zirconium dissolved in magma, not by degradation of some older Zr-mineral, redeposition, and new crystallization.

Although some discrepancies exist between the original interpretations of the sources of the studied plutons [45,46,70,71], the existence of two distinct groups of peralkaline rocks differing also in the shapes and chemistries of their zircons is evident.

Two kinds of peralkaline syenites differing in assemblages of Zr and Ti minerals is well known and termed as miaskitic (zircon + titanite) vs. agpaitic (complex Zr, Ti, Nb-silicates). Marks et al. [72] proposed to apply this terminology also to peralkaline granites. Following this proposal, the studied strongly peralkaline rocks with dominant secondary zircon should be classified as agpaitic, while the mildly peralkaline granites with exclusively primary zircon as miaskitic.

### 5.2. Relation between Zircon Chemistry and Texture

While primary magmatic zircon from F-rich peralkaline systems at Madeira and Ivigtut have generally monotonous textures (euhedral crystals) and chemistries, a wide range of textural varieties differing in chemical composition were found at Khan Bogd and Khalzan Buregte (Figure 8).

For example, globular zircon from relative less altered Px-granite from Khan Bod (#KB3, EGD09-256, Figure 3e) is rich in Y and Nb, thus resembling euhedral-subhedral zircon crystals from the same samples (Figure 8a,b). Globular zircon of the same appearance from the strongly metasomatized facies of this granite (#KB4, Figure 3f) is poor in both elements. Radiating zircon aggregates from ekerite (#KB13) are rich in Y but poor in Nb. And the unusual form of zircon, i.e. rounded admixtures in porous hematite (or pseudomorph of magmatic magnetite), is surprisingly chemically similar to primary magmatic zircon.

At Khalzan Buregte, zircons from both suites can be clearly distinguished from each other based on their Y/Yb values (Figure 8c). Aggregates of hydrothermal zircon, similarly to scarce primary-looking crystals, show a large dispersion of non-formula elements contents; i.e., no striking relation between the shape (manner of origin) and chemical composition exists. Nevertheless, all zircons from the older suite have identical, low, “primitive” Y/Yb ratios of ca. 10/1, and the relatively highest Y values correlate with the highest Nb in all textural types (Figure 8d).

Enrichment in LREE was recognized as a common consequence of metamictization (up to 0.99 wt% Ce<sub>2</sub>O<sub>3</sub> [20]) and as a reliable indicator of hydrothermal alteration of apparently pristine magmatic zircons (up to ca. 2000 ppm Ce) [19]. We found in rocks

of the Khalzan Buregte older suite up to 0.04 wt%  $\text{Ce}_2\text{O}_3$  in radial zircon aggregates (Figure 3b) and up to 0.21 wt%  $\text{Ce}_2\text{O}_3$  in globular aggregates (Figure 3e) within fully disintegrated silicates. An extreme content up to 18 wt%  $\text{Ce}_2\text{O}_3$  represents already a zircon-REE transitional phase or cryptocrystalline mixture of zircon and a LREE-phase in association with xenotime in a pyroxene syenite (Figure 3g). All mentioned Ce-rich aggregates are poor in La (below the detection limit of EPMA) indicating strongly oxidizing environment during zircon precipitation.

Zircon crystals from the younger suite are irregularly but significantly enriched in Hf, Yb, U, and Th, resembling zircons from the Madeira pluton.

Nearly all Khalzan Buregte zircons are characterized by low totals and enrichment in non-formula elements Al, Ca, and Fe. In the younger suite, Ca and Al enrichment correlates with the enrichment in radioactive elements U and Th (Figure 8e) and should be explained by a radioactive damage of the zircon structure [63]. Zircons from the older suite, although free of U and Th, also show very high contents of non-formula elements and low analytical totals. This lack of mass must have another explanation, most probably a high amount of micropores resulting from hydrothermal precipitation (compare [21]). In any case, two styles of hydrothermal zircon origin/alteration can be recognized here: (i) one with fluids rich in Nb, Ce, and Y, vs. (ii) one with fluids free of all traces. This may indicate variable source/composition/temperature of post-magmatic fluids leading to different secondary mineral assemblages. Strong complexation is required for the effective transport of Zr in the fluid. At low F contents, NaOH or  $\text{CO}_2$  can play a role in particular [73] and thus affect the association of simultaneously transported elements. The alteration of primary Na-zirconosilicates to zircon may take place gradually with an intermediate stage of Ca-zirconosilicates [35,67]. It was not possible to distinguish such gradual processes in our samples due to the high intensity of alteration. To generalize somewhat, hydrothermally altered zircons can vary significantly in absolute abundances of non-formula elements, but Zr/Hf and Y/Yb values remain the same as rare primary zircon grains.

### 5.3. Low Analytical Totals

Zircons enriched in radioactive elements U and Th often show low analytical totals and contain substantial amounts of non-formula elements like Al, Ca, Fe, and Mn. This is usually explained as a result of metamictization, i.e., radioactive damage of the zircon structure [20,63]. Such an explanation is applicable to U, Th-enriched zircons with low analytical totals from Madeira and the younger suite of Khalzan Buregte, but not to the U, Th-free globular zircon crystals from Khan Bogd and Khalzan Buregte. Zircon globules of similar shape and size (70  $\mu\text{m}$ ), and analytical totals down to 95.9 wt% found Vlach in Corupá pluton, Brazil [21]. Unlike globules from Khan Bogd, these are enriched, compared to primary zircon, not only with Al, Ca, Fe, and Mn, but also with REE, especially with LREE, and are interpreted to grow in a low-temperature oxidizing environment [21]. Presumably, the discussed late globular zircons are very similar to low-temperature globular “hydrozircon” from sandstone-type uranium deposits of Břevniště, Czech Republic, with analytical totals dropping to 80 wt% [74]. In the case of such low totals, any calculation of formula proportions is risky; nevertheless, element ratios can be determined correctly. In the hydrozircon from Břevniště, Zr clearly predominates over Si, and a substitution reaction  $\text{SiO}_4 \leftrightarrow (\text{OH})_4$  can be expected. By contrast, Zr and Si contents in globular zircon from the studied peralkaline granitoids and those referred by [21] are about equal (in apfu), which makes any extensive hydration improbable. The possible explanation is therefore the presence of a large number of micropores or the amorphous state of the material. In any case, this problem calls for a further, more detailed study of the crystal structure.

### 5.4. Zirconium–Hafnium Ratio

The Zr/Hf values by weight are 33–38 in chondrites [75,76], 37 in primitive mantle [43], and 36 in the upper continental crust [44]. This implies that the Zr/Hf fractionation among these reservoirs is negligible. Nevertheless, Zr/Hf values in mineral zircon vary

considerably. A general rule is that the Zr/Hf value decreases with a progressive fractionation of the melt. The content of Hf in zircons from rocks ranging from kimberlites to common granites remains stable (0.8–1.7 wt% HfO<sub>2</sub>), but increase significantly in strongly fractionated granites [10,77]. Kempe et al. [78] pointed out that an extreme Hf enrichment is typical of zircons with a patchy structure from P-poor (more commonly A-type) granites; they interpreted that zircon crystals with Hf-rich rims around Hf-poorer cores were as a result of hydrothermal replacement. Nevertheless, Linnen and Keppler [79] experimentally proved the possibility of a strong Hf enrichment, i.e., Zr/Hf value reduction, through pure magmatic fractionation. Moreover, intensity of fractionation depends on the composition of the melt: the molar zircon/hafnon solubility ratio in strongly peralkaline melt is close to unity, while in metaluminous melt, it is 0.2 [79]. Thus, the late intrusive phases of metaluminous/peraluminous suites, unlike peralkaline ones, are able to reach strong Hf-enrichment.

The atomic Zr/Hf values in the studied peralkaline zircon crystals vary from ca. 80 to 100 at Khan Bogd and in the mineralized domains of the older suite of Khalzan Buregte [36] across 60–80 in the older suite of Khalzan Buregte and 30–50 at Ivigtut to 10–20 at Madeira and in the younger suite of Khalzan Buregte. The Nb–Zr–REE-mineralized plutons at Strange Lake and Thor Lake [33,35,37] contain zircons with atomic Zr/Hf near 60. The atomic Zr/Hf value in chondrites equals 74, i.e., zircon from strongly peralkaline Px-bearing granitoids shows chondritic to slightly subchondritic values (compare Table S2), indicating a geochemically primitive source. On the other hand, F-rich mildly peralkaline rocks are products of long-lasting intensive Zr/Hf fractionation.

#### 5.5. Hf/Y Antagonism

Already, Pupin [9] had drawn attention to this feature potentially discriminating zircon from peralkaline rocks (Y-enriched at low Hf) from zircon from evolved peraluminous granites (Hf-enriched at low Y). Pupin characterized zircon from peralkaline granitoids as having <1.1 wt% HfO<sub>2</sub> and 0.5–1.5 wt% Y<sub>2</sub>O<sub>3</sub>. Our data from Px-bearing strongly peralkaline rocks agree with low Hf (~1 wt% HfO<sub>2</sub>) but expand the Y range to 0–9 wt% Y<sub>2</sub>O<sub>3</sub>. Mica-bearing F-rich mildly peralkaline rocks from Madeira and Ivigtut contain zircons rich in Hf (2–13 wt% HfO<sub>2</sub>) with low to moderate Y-contents (<1.5 wt% Y<sub>2</sub>O<sub>3</sub>). Compared with the large datasets of zircon from S- and A-type granites, we see very similar shapes of distribution and ranges of Hf and Y contents in all types of granitoids (Figure 6d), indicating only limited usefulness of the discrimination scheme proposed by [21].

#### 5.6. Y/HREE Fractionation

Values of the relative ratios between Y and HREE, best represented by Ho, remain the same through the majority of geological processes including the fractional crystallization of common granitoids. The reasons for this are the almost identical values of charge (3+), electronegativity (1.11), and ionic radii (1.019 vs. 1.015 Å) [80]. Only during the final stage of fractionation of fluid-enriched granitic melt and during the magmatic/hydrothermal transition, Y tends to be better complexed and segregated into fluid. Usually, this process is expressed by a decrease in the Y/Ho value, which is normally (chondrite, mantle, crust) ~29 by weight [81]. Since Ho contents in zircon are usually too low to be analyzed using EPMA, we use a proxy value of Y/Yb, which equals to 9.75 by weight in standard conditions [81] (Table S2), i.e., ca. 20 by atoms, and the Y<sub>2</sub>O<sub>3</sub>/Yb<sub>2</sub>O<sub>3</sub> value should equal 8.95 (Figure 9a). At the same time, the Y/HREE ratio in zircon, apparently expressed as Y<sub>2</sub>O<sub>3</sub>/Yb<sub>2</sub>O<sub>3</sub>, is typical for each pluton/rock type and varies from ca. 10 (i.e., near-chondritic values) in strongly peralkaline plutons (Khan Bogd, older suite of Khalzan Buregte) to <1 at Madeira.

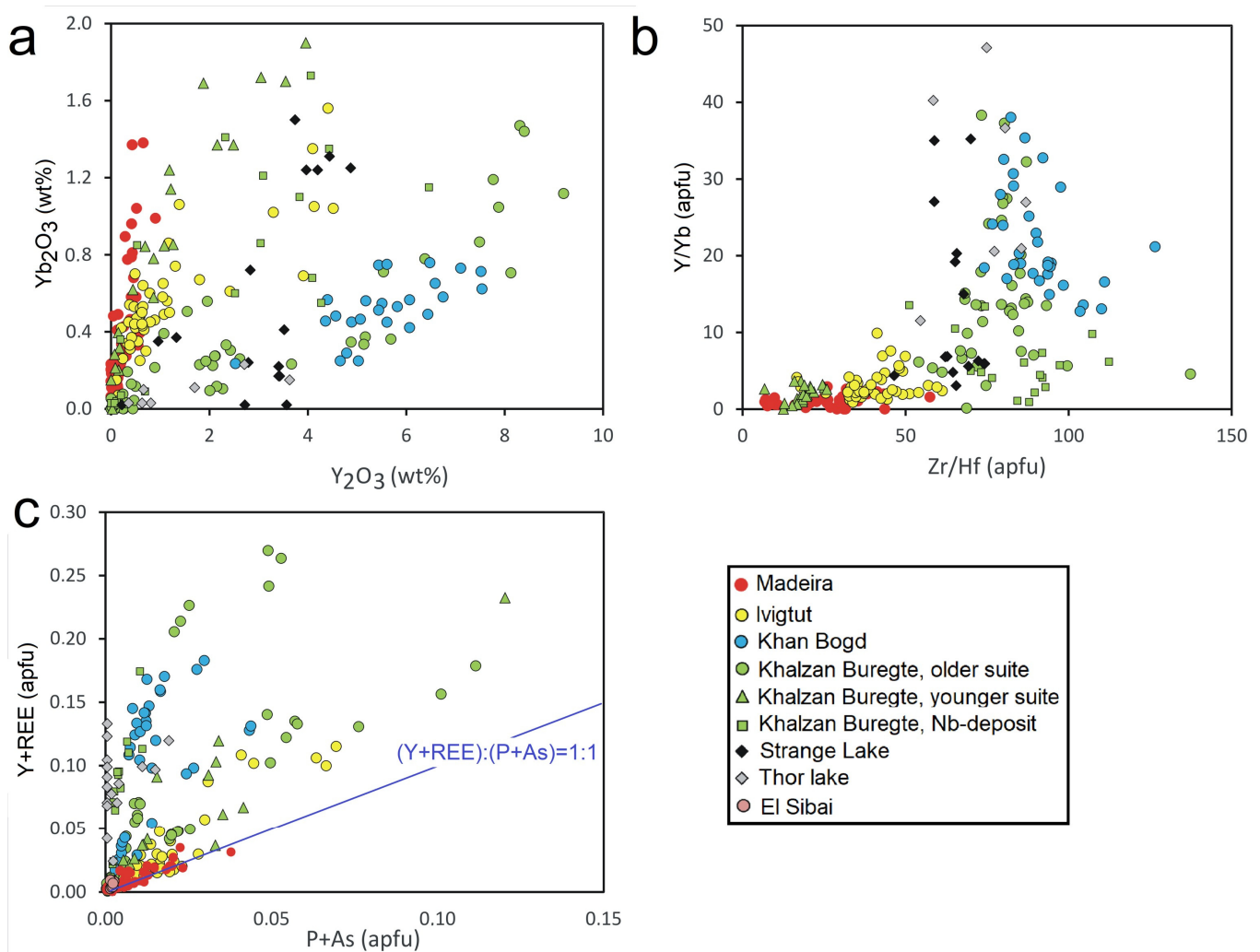


**Figure 9.** Chemical composition of studied zircons: (a)  $Y_2O_3$  vs.  $Yb_2O_3$ ; (b)  $Zr/Hf$  vs.  $Y/Yb$ ; (c)  $P + As$  vs.  $Y + REE$ .

The  $Y/Yb$  value in zircon decreases in a similar way as the  $Zr/Hf$  value during magma evolution [82], well discriminating zircons from strongly peralkaline P<sub>x</sub>-bearing rocks ( $Zr/Hf$  almost always >70,  $Y/Yb$  mostly >5) from those from F-saturated mildly peralkaline magmas ( $Zr/Hf$  < 70,  $Y/Yb$  < 5, Figure 9b).

### 5.7. Relation between $Y + REE$ and $P$ Contents in Zircon

Mineral xenotime  $(Y,REE)PO_4$  is isostructural to zircon, and zircon is able to incorporate a substantial amount of xenotime component [30,64]. In such a case, the atomic ratio between  $P$  and  $Y + REE$  should equal 1 (Figure 9c). In the studied zircon samples, only analyses from Madeira and part of the analyses from Ivigtut meet this premise. In most other analyses, the  $(Y + REE)$ -to- $P$  ratio is much higher indicating a lack of  $P$  in the crystallizing system. And indeed, all studied peralkaline rocks contain a maximum of only 0.05%  $P_2O_5$ . In contrast, peraluminous rocks typically contain 0.2% or more  $P_2O_5$ , and zircon from such rocks contains ideal xenotime molecules as expected [3,16].

Another mechanism of  $Y + REE$  incorporation into the zircon lattice must play a major role in case of zircons from peralkaline melt. While the content of  $Nb + Ta$  is usually much lower than the content of  $Y + REE$ , the substitution  $(Nb + Ta)^{5+} + (Y + REE)^{3+} \leftrightarrow Zr^{4+} + Zr^{4+}$  cannot play an important role. Here, the hydrogenation of oxygen, i.e.,  $Zr + O \leftrightarrow REE + OH$ , is probably the prevailing mechanism.

### 5.8. Zircon-like Transitional Phases (Solid Solutions)

Förster [30] described Th-, U-, and Y-rich zircon and intermediate solid solutions in the zircon–xenotime–thorite–coffinite system from A-type granites in the eastern Erzgebirge (Germany) and Jordan. Breiter et al. [64] reported a nearly continuous mixing series between zircon and thorite/coffinite and between zircon and xenotime/chernovite from Hora sv. Kateřiny in the Erzgebirge. In the studied peralkaline zircon crystals, the tendency to form mixed compositions is much smaller. Max. 4% of the thorite/coffinite component were found in several grains from the younger suite at Khalzan Buregte, and about 15% of the xenotime component were found in zircon from Khan Bogd. Similar contents of the xenotime component were also reported from the REE–Zr–Nb-mineralized Strange Lake and Thor Lake plutons and from mineralized domains within the older suite of Khalzan Buregte [33,35,36].

A highly unusual transitional composition with 0.35–0.40 apfu Zr, 0.20 apfu Y, 0.25 apfu Ce, 0.4 apfu Si, 0.05 apfu P, 0.15 apfu Ti, and some Ca was found at Khalzan Buregte. A quite homogeneous composition of these mineral grains was proved by several spot analyses (Figure 3g).

### 5.9. Are There Specific Chemical Features of Zircon from Peralkaline Granitoids Compared to Zircons from A- and S-Type Granites?

As already shown in Figures 6–9 and discussed above, zircon from peralkaline rocks shows a specific chemical composition. The contents of most chemical elements and elemental ratios in zircons from particular rocks types, i.e., strongly peralkaline Px-bearing granites and syenites, and mildly peralkaline Px + Mca-bearing granites, are shown in Table 5, together with representative zircon values for strongly peraluminous S-type granites and mildly peraluminous A-type granites. The highest median of HfO<sub>2</sub> was found in zircon from mildly peralkaline granites, while the highest contents of U and Th were found in A-type granites, and the highest P contents in S-type granites. Hydrothermal zircon from strongly peralkaline granites and syenites typically shows the highest contents of Y and the lowest medians of analytical totals.

**Table 5.** Medians of contents of significant minor elements (wt%) and element ratios (in apfu) in zircon of different affiliation. (Here, it should be noted that the values are somewhat affected by the different representation of common vs. highly fractionated rock in individual datasets.)

Rock Type	Mildly Peralkaline	Strongly Peralkaline	S-Type Granites	A-Type Granites
Principal Origin of Zircon	Mostly Magmatic	Mostly Hydrothermal	Magmatic	Magmatic
n	106	105	432	268
HfO <sub>2</sub>	3.2	1.14	1.71	1.81
Y <sub>2</sub> O <sub>3</sub>	0.42	2.27	0.16	0.55
Yb <sub>2</sub> O <sub>3</sub>	0.44	0.55	0.025	0.31
ThO <sub>2</sub>	0.1	0.13	0.03	0.24
UO <sub>2</sub>	0.05	0.15	0.51	0.62
TiO <sub>2</sub>	bdl	0.12	0.01	0.01
P <sub>2</sub> O <sub>5</sub>	0.38	0.33	0.84	0.33
Analytical total	99.03	93.83	97.36	95.75
Zr/Hf	33	80	60	53
Y/Yb	1.6	12.3	6.1	3.6
U/Th	0.49	0.7	7.9	1.8

Note: bdl—below detection limit.

A detailed comparison of the relationship between shape, relative timing of crystallization, and chemistry of zircon from peralkaline granites and quartz-bearing syenites showed that the main chemical zircon values (Zr/Hf, Y/Yb) are completely characteristic for each group of rocks, this is mildly vs. strongly peralkaline, independent of the zircon

texture and timing of crystallization. The U/Th value has a large and difficult-to-interpret dispersion (Figure 10a).

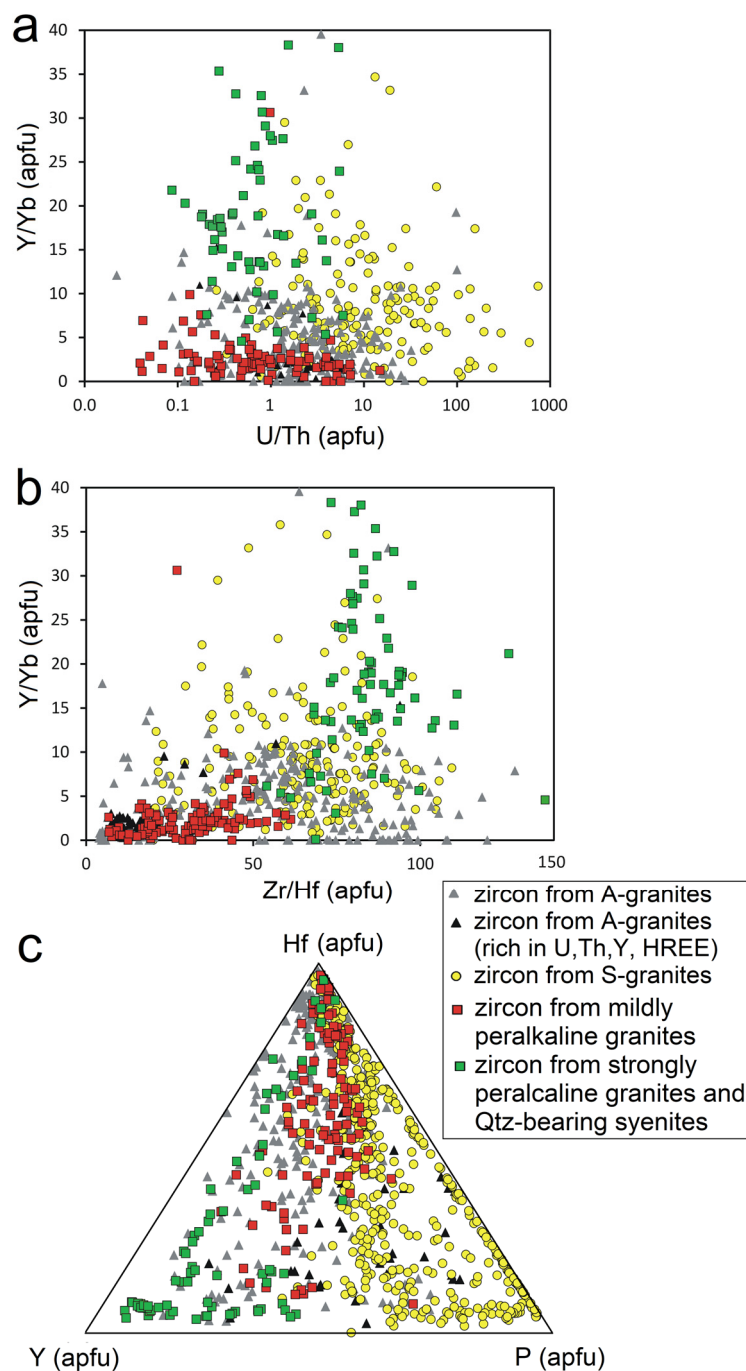


**Figure 10.** Discrimination of zircon from different types of granitoids: (a) U/Th vs. Y/Yb, (b) Zr/Hf vs. Y/Yb, and (c) ternary diagram Y-Hf-P (all in atoms per formula unit).

Although the differences in some values in zircon chemistry seem to be large (Table 5), graphic discrimination of individual types of zircon is, due to wide dispersions of all parameters, not simple [3,10,16,22]. Along contents and distribution patterns of REE [3,22], which, however, cannot be fully determined using EPMA, the Zr/Hf, and Y/Yb values seem to be the relatively best option (Figure 10b).

Magmatic zircon from mildly peralkaline granites forms relatively compact fields of projective points with low Y/Yb (mostly <5) and Zr/Hf decreasing via fractional crystal-

lization to less than 10 in extreme cases; U/Th values range between 0.05 and 10, without any correlation to Zr/Hf. The hydrothermal zircons from strongly peralkaline rocks generally differ in higher Zr/Hf (mostly >60) and Y/Yb (mostly >10) and lower U/Th (mostly <1). Composition of zircon from metaluminous A-type granites closely resembles those of magmatic zircon from mildly peralkaline rocks with somewhat larger dispersion in direction to higher Zr/Hf and Y/Yb values. Chemical variability of zircon from S-type granites is even larger corresponding to the great variability of the parent peraluminous rocks involved to data collection.

The Y-Hf-P ternary diagram (Figure 10c) depicts some relations among composition of zircon, composition of parental rocks, and coexisting mineral assemblage. The diagram highlights common enrichment in phosphorus in zircon from typically P-rich and Th-, Y-, and REE-poor S-type granites [31]. Zircon from P-poor Th-, Y-, REE-enriched mildly peralkaline granites commonly associated with contemporaneous thorite, but xenotime is scarce in this assemblage; this implies the dominance of Y over Th and P in the zircon. Zircons from strongly peralkaline granites/syenites and from A-type granites are dispersed through the whole diagram. Strongly evolved zircons from all rock types meet at the Hf-apex.

Figure 10 also highlights the relative dispersion in the composition of intermediate phases among zircon, xenotime, thorite, and coffinite from A-type granites [30] which more less resemble the dispersion of “common” zircons from A-type granites with only a small shift to higher Y and P content (xenotime component).

## 6. Conclusions

The studied plutons are classified into two geochemically distinct groups: (i) mildly peralkaline granite plutons at Ivigtut and Madeira, and the younger suite of Khalzan Buregte, and (ii) strongly peralkaline granite and syenite plutons at Khan Bogd and the older suite of Khalzan Buregte. These two rock groups correspond to two contrasting types of zircon mineralogy:

- The mildly peralkaline granites, containing small amounts of Fe-mica along the Napyroxene, are enriched in fluorine, and contain Hf-, U-, and Th-rich zircon as the exclusive primary Zr mineral. This zircon was sometimes metamictized and enriched in non-formula elements Al, Ca, and Fe, but not dissolved, transported, and reprecipitated;
- The strongly peralkaline rock contain none or only little magmatic zircon; the dominant primary carriers of zirconium were different zirconosilicates. During post-magmatic hydrothermal stage, zirconosilicates were altered and, almost without relicts, replaced by secondary zircon aggregates and a mixture of different allumosilicates, carbonates, and Fe-oxides/hydroxides.

While primary magmatic zircon from mildly peralkaline systems always forms euhedral crystals of monotonous or only indistinctly zonal chemistry, a wide range of textural varieties of hydrothermal zircon, i.e., radial, globular, and vein-like, with variable chemical composition were found in strongly peralkaline rocks. Nearly all hydrothermal zircon aggregates are characterized by low totals; this lack of mass most probably reflects a high amount of micropores resulting from hydrothermal precipitation. Great variability in non-formula element (Al, Ca, Fe, Nb, Ce, Y) contents, regardless of texture, indicates the variable source/composition/temperature of post-magmatic fluids leading to different secondary mineral assemblages.

Zircon chemical values Zr/Hf and Y/Yb are completely characteristic for each group of rocks, which is mildly vs. strongly peralkaline, independent of the zircon texture and timing of crystallization, and can be used for their classification. While hydrothermal (+rare magmatic) zircon from strongly peralkaline rocks exhibits primitive (mantle-like) values (Y/Yb > 5, mostly >10; Zr/Hf > 60), magmatic zircon from mildly peralkaline rocks has evolved to extremely evolved values (Y/Yb < 5, Zr/Hf < 50 up to <10). The difference in both values mirrors the different bulk-rock composition, i.e., the manner of fractional crystallization and content of water and fluxing elements in both contrasting rock suites.

Relative zircon enrichment in Y, REE, Th, or P refers to the composition of parental rock and/or assemblage of Y-, REE-, Th-, and U-bearing phases.

**Supplementary Materials:** The following supporting information can be downloaded at: <https://www.mdpi.com/article/10.3390/min14020187/s1>. Table S1: Basic description of samples; Table S2: Important geochemical values.

**Author Contributions:** Conceptualization, K.B.; methodology, K.B. and Z.K.; investigation, K.B. and J.K.; analyzes Z.K.; writing—original draft preparation, K.B.; writing—review and editing, K.B.; supervision, J.K.; funding acquisition, J.K. All authors have read and agreed to the published version of the manuscript.

**Funding:** This study was supported by the Czech Science Foundation Project No. EXPRO 19-29124X.

**Data Availability Statement:** The primary data are available upon request at the authors, due to privacy.

**Acknowledgments:** Detail inspirational review by W.J. Collins and one anonymous reviewer are acknowledged with pleasure.

**Conflicts of Interest:** Authors Karel Breiter and Jindřich Kynický, are employees of company BIC Brno Ltd., but did not receive a funding from the company. Therefore, the paper reflects the views of these scientists and not the company. The remaining author also declare that no conflicts of interest since the funders (Czech Science Foundation) had no role in the design of the study; in the collection, analyses, or interpretation of data; in the writing of the manuscript; or in the decision to publish the results.

## References

1. Speer, J.A. Zircon. *Rev. Mineral.* **1980**, *5*, 67–112.
2. Deer, W.A.; Howie, R.A.; Zussman, J. *Rock-Forming Minerals*; The Geological Society: London, UK, 1997.
3. Hanchar, J.M.; Hoskin, P.W.O. Zircon. *Rev. Miner. Geochem.* **2003**, *53*, 1–500.
4. Davis, D.W.; Krogh, T.E.; Williams, I.S. Historical development of zircon geochronology. *Rev. Miner. Geochem.* **2003**, *53*, 145–181. [[CrossRef](#)]
5. Hanchar, J.M.; Watson, E.B. Zircon saturation thermometry. *Rev. Miner. Geochem.* **2003**, *53*, 89–112. [[CrossRef](#)]
6. Fedo, C.M.; Sircombe, K.N.; Rainbird, R.H. Detrital zircon analysis of the sedimentary record. *Rev. Miner. Geochem.* **2003**, *53*, 277–303. [[CrossRef](#)]
7. Kinny, P.D.; Maas, R. Lu–Hf and Sm–Nd isotope systems in zircon. *Rev. Miner. Geochem.* **2003**, *53*, 327–341. [[CrossRef](#)]
8. Du, B.; Yang, Z.; Yang, L.; Chen, Q.; Zhu, J.; Shi, K.; Li, G.; Wang, L.; Lu, J. Zircon Hf-isotopic mapping applied to the metal exploration of the Sanjiang Tethyan orogenic belt, southwestern China. *Appl. Sci.* **2002**, *12*, 4081. [[CrossRef](#)]
9. Pupin, J.-P. Zircon and granite petrology. *Contrib. Mineral. Petrol.* **1980**, *73*, 207–220. [[CrossRef](#)]
10. Belousova, E.A.; Griffin, W.L.; O'Reilly, S.Y.; Fisher, N.I. Igneous zircon: Trace element composition as an indicator of source rock type. *Contrib. Mineral. Petrol.* **2002**, *143*, 602–622. [[CrossRef](#)]
11. Pupin, J.-P. Granite genesis related to geodynamics from Hf–Y in zircon. *Transact. R. Soc. Edinburg Earth Sci.* **2000**, *91*, 245–256.
12. Grimes, C.B.; John, B.E.; Kelemen, P.B.; Mazdab, F.K.; Wooden, J.L.; Cheadle, M.J.; Hangoj, K.; Schwartz, J.J. Trace element chemistry of zircon from oceanic crust: A method for distinguishing detrital zircon provenance. *Geology* **2007**, *35*, 643–646. [[CrossRef](#)]
13. Grimes, C.B.; Wooden, J.L.; Cheadle, M.J.; John, B.E. Fingerprinting tectono-magmatic provenance using trace elements in igneous zircon. *Contrib. Mineral. Petrol.* **2015**, *170*, 1–26.
14. Kirkland, C.L.; Smithies, R.H.; Taylor, R.J.M.; Evans, N.; McDonald, B. Zircon Th/U ratios in magmatic environs. *Lithos* **2015**, *212–215*, 397–414. [[CrossRef](#)]
15. Hoskin, P.W.O.; Ireland, T.R. Rare earth element chemistry of zircon and its use as a provenance indicator. *Geology* **2000**, *28*, 627–630. [[CrossRef](#)]
16. Breiter, K.; Lamarao, C.N.; Borges, R.M.K.; Dall'Agno, R. Chemical characteristic of zircon from A-type granites and comparison to zircon of S-type granites. *Lithos* **2014**, *192–195*, 208–225. [[CrossRef](#)]
17. Nardi, L.V.S.; Formoso, M.L.L.; Müller, I.F.; Fontana, E.; Jarvis, K.; Lamarão, C. Zircon/rock partition coefficients of REEs, Y, Th, U, Nb, and Ta in granitic rocks: Uses for provenance and mineral exploration purposes. *Chem. Geol.* **2013**, *335*, 1–7. [[CrossRef](#)]
18. Padilla, A.J.; Gualda, G.A.R. Crystal-melt elemental partitioning in silicic magmatic systems: An example from the peach Spring Tuff high-silica rhyolite, Southwest USA. *Chem. Geol.* **2016**, *440*, 326–344. [[CrossRef](#)]
19. Bell, E.A.; Boehnke, P.; Barboni, M.; Harrison, T.M. Tracking chemical alteration in magmatic zircon using rare earth element abundances. *Chem. Geol.* **2019**, *510*, 56–71. [[CrossRef](#)]

20. Kubeš, M.; Leichmann, J.; Wertich, V.; Mozola, J.; Holá, M.; Kanický, V.; Škoda, R. Metamictization and fluid-driven alteration triggering massive HFSE and REE mobilization from zircon and titanite: Direct evidence from EMPA imaging and LA-ICP-MS analyses. *Chem. Geol.* **2021**, *586*, 120593. [[CrossRef](#)]
21. Vlach, S.R.F. On the morphology and geochemistry of hydrothermal crypto- and microcrystalline zircon aggregates in a peralkaline granite. *Minerals* **2022**, *12*, 628. [[CrossRef](#)]
22. Hoskin, P.W.O.; Schaltegger, U. The composition of zircon and igneous and metamorphic petrogenesis. *Rev. Miner. Geochem.* **2003**, *53*, 27–62. [[CrossRef](#)]
23. Breiter, K.; Müller, A.; Shail, R.; Simons, B. Composition of zircons from the Cornubian Batholith of SW England and comparison with zircons from other European Variscan rare-metal granites. *Mineral. Mag.* **2016**, *80*, 1273–1289. [[CrossRef](#)]
24. Wang, R.C.; Fontan, F.; Xu, S.J.; Chen, X.M.; Monchoux, P. Hafnian zircon from the apical part of the Suzhou granite, China. *Canad. Mineral.* **1996**, *34*, 1001–1010.
25. Wang, R.C.; Zhao, G.T.; Lu, J.J.; Chen, X.M.; Xu, S.J.; Wang, D.Z. Chemistry of Hf-rich zircons from the Laoshan I- and A-type granites, Eastern China. *Mineral. Mag.* **2000**, *64*, 867–877. [[CrossRef](#)]
26. Wang, R.C.; Fontan, F.; Monchoux, P. Minéraux disséminés comme indicateurs du caractère pegmatitique du granite de Beauvoir, Massif d'Échassières, Allier, France. *Canad. Mineral.* **1992**, *30*, 763–770.
27. Wang, X.; Griffin, W.L.; Chen, J. Hf contents and Zr/Hf ratios in granitic zircons. *Geochem. J.* **2010**, *44*, 65–72. [[CrossRef](#)]
28. Correia Neves, J.M.; Lopes Nunes, J.E.; Sahama, T.G. High hafnian members of the zircon-hafnon series from the granite pegmatites of Zambézia, Mozambique. *Contrib. Mineral. Petrol.* **1974**, *48*, 73–80. [[CrossRef](#)]
29. Yin, R.; Wang, R.C.; Zhang, A.C.; Hu, H.; Zhu, J.C.; Rao, C.; Zhang, H. Extreme fractionation from zircon to hafnon in the Koktokay No.1 pegmatite, Altai, Northwestern China. *Am. Mineral.* **2013**, *98*, 1714–1724. [[CrossRef](#)]
30. Förster, H.-J. Composition and origin of intermediate solid solutions in the system thorite-xenotime-zircon-coffinite. *Lithos* **2006**, *88*, 35–55. [[CrossRef](#)]
31. Breiter, K.; Förster, H.-J.; Škoda, R. Extreme P-, Bi-, Nb-, Sc-, U- and F-rich zircon from fractionated perphosphorus granites: The peraluminous Podlesí granite system, Czech Republic. *Lithos* **2006**, *88*, 15–34. [[CrossRef](#)]
32. Kynický, J.; Chakhmouradian, A.R.; Xu, C.; Krmíček, L.; Galiová, M. Distribution and evolution of zirconium mineralization in peralkaline granites and associate pegmatites of the Khan Bogd complex, Southern Mongolia. *Canad. Mineral.* **2011**, *49*, 947–965. [[CrossRef](#)]
33. Sheard, E.R.; Williams-Jones, A.E.; Heiligmann, M.; Pederson, C.; Trueman, D.L. Controls on the concentration of zirconium, niobium, and the rare earth elements in the Thor Lake rare metal deposit, Northwest Territories, Canada. *Econ. Geol.* **2012**, *107*, 81–104. [[CrossRef](#)]
34. Kempe, U.; Möckel, R.; Graupner, T.; Kynický, J.; Dombon, E. The genesis of Zr-Nb-REE mineralisation at Khalzan Buregte (Western Mongolia) reconsidered. *Ore Geol. Rev.* **2015**, *64*, 602–625. [[CrossRef](#)]
35. Gysi, A.P.; Williams-Jones, A.E.; Collins, P. Lithochemical vectors for hydrothermal processes in the Strange Lake peralkaline granitic REE-Zr-Nb deposit. *Econ. Geol.* **2016**, *111*, 1241–1276. [[CrossRef](#)]
36. Sarangua, N.; Watanabe, Y.; Echigo, T.; Hoshino, M. Chemical characteristic of zircon from Khaldzan Burgedei peralkaline complex, Western Mongolia. *Minerals* **2019**, *9*, 10. [[CrossRef](#)]
37. Smith, D.G.W.; de St. Jorre, L.; Reed, S.J.B.; Long, J.V.P. Zonally metamictized and other zircons from Thor Lake, Northwest Territories. *Canad. Mineral.* **1991**, *29*, 301–309.
38. Xie, L.; Wang, R.; Chen, X.; Qui, J.; Wang, D. Th-rich zircon from peralkaline A-type granite: Mineralogical features and petrological implications. *Chin. Sci. Bull.* **2005**, *50*, 809–817.
39. Nardi, L.V.S.; Formoso, M.L.L.; Jarvis, K.; Oliveira, L.; Bastos Neto, A.C.; Fontana, E. REE, Y, Nb, U, and Th contents and tetrad effect in zircon from a magmatic–hydrothermal F-rich system of Sn-rare metal-cryolite mineralized granites from the Pitinga Mine, Amazonia, Brazil. *J. S. Am. Earth Sci.* **2012**, *33*, 34–42. [[CrossRef](#)]
40. Vilalva, F.C.J.; Simonetti, A.; Vlach, S.R.F. Insights on the origin of the Graciosa A-type granites and syenites (Southern Brazil) from zircon U-Pb geochronology, chemistry, and Hf and O isotope compositions. *Lithos* **2019**, *340–341*, 20–33. [[CrossRef](#)]
41. Shand, S.J. Eruptive Rocks. In *Their Genesis Composition Classification, and their Relation to Ore-Deposits*; John Wiley & Sons: New York, NY, USA, 1943.
42. Loiselle, M.C.; Wones, D. Characteristics and origin of anorogenic granites. *Geol. Soc. Am. Abstr. Programs* **1979**, *11*, 468.
43. Lyubetskaya, T.; Korenga, J. Chemical composition of Earth's mantle and its variance. *J. Geophysic. Res.* **2007**, *112*, B03211.
44. Rudnick, R.L.; Gao, S. Composition of the continental crust. *Treatise Geochem.* **2003**, *3*, 1–64.
45. Eby, G.N. Chemical subdivision of the A-type granitoids: Petrogenetic and tectonic implications. *Geology* **1992**, *20*, 641–644. [[CrossRef](#)]
46. Kovalenko, V.I.; Tsaryeva, G.M.; Goreglyad, A.V.; Yarmolyuk, V.V.; Troitsky, V.A. The peralkaline granite-related Khaldzan-Buregtey rare metal (Zr, Nb, REE) deposit, Western Mongolia. *Econ. Geol.* **1995**, *90*, 530–547. [[CrossRef](#)]
47. Costi, H.T.; Dall'Agnol, R.; Moura, C.A.V. Geology and Pb-Pb geochronology of Paleoproterozoic volcanic and granitic rocks of Pitinga province, Amazonian craton, northern Brazil. *Int. Geol. Rev.* **2000**, *42*, 832–849. [[CrossRef](#)]
48. Goodenough, K.M.; Upton, B.G.J.; Ellam, R.M. Geochemical evolution of the Ivigtut granite, South Greenland: A fluorine-rich "A-type" intrusion. *Lithos* **2000**, *51*, 205–221. [[CrossRef](#)]

49. Paludo, C.M.; Bastos Neto, A.C.; Pereira, V.P.; Botelho, N.F. Mineralogia e geoquímica de pegmatitos ricos em ETR, F e metais alcalinos associados a facies albíta granito no depósito de Sn-Nb-Ta- (F, ETR, U, Th) Madeira (mina Pitinga, AM, Brasil). *Pesquisas Em Geociências* **2018**, *45*, e0747.
50. Kovalenko, V.I.; Yarmolyuk, V.V.; Sal'nikova, E.B.; Kozlovsky, A.M.; Kotov, A.B.; Kovach, V.P.; Savatenkov, V.M.; Vladykin, N.V.; Ponomarchuk, V.A. Geology, geochronology, and geodynamics of the Khan Bogd alkali granite pluton in Southern Mongolia. *Geotectonics* **2006**, *40*, 450–466. [[CrossRef](#)]
51. Pauly, H.; Bailey, J.C. Genesis and evolution of the Ivigtut cryolite deposit, SW Greenland. *Meddelelser Om Gronl. Geosci.* **1999**, *37*, 1–60. [[CrossRef](#)]
52. Köhler, J.; Schönerberger, J.; Upton, B.; Markl, G. Halogen and trace-element chemistry in the Gardar province, South Greenland: Subduction-related mantle metasomatism and fluid exsolution from alkalic melts. *Lithos* **2009**, *113*, 731–747. [[CrossRef](#)]
53. Costi, H.T.; Dall'Agnol, R.; Pichavant, M.; Ramo, O.T. The peralkaline tin-mineralized Madeira cryolite albite-rich granite of Pitinga, Amazonian craton, Brazil: Petrography, mineralogy and crystallization processes. *Canad. Mineral.* **2009**, *47*, 1301–1327. [[CrossRef](#)]
54. Bastos Neto, A.C.; Pereira, V.P.; Ronchi, L.H.; Lima, E.F.; Frantz, J.C. The world-class Sn, Nb, Ta, F (Y, REE, Li) deposit and the massive cryolite associated with the albite-enriched facies of the Madeira A-type granite, Pitinga mining district, Amazonas State, Brazil. *Can. Mineral.* **2009**, *47*, 1329–1357. [[CrossRef](#)]
55. Sami, M.; Osman, H.; Ahmed, A.F.; Zaky, K.S.; Abart, R.; Sanislav, I.V.; Abdelrahman, K.; Fnais, M.S.; Xiao, W.; Abbas, H. Magmatic evolution and rare metal mineralization in Mount El-Sibai peralkaline granites, central Eastern Desert, Egypt: Insights from whole-rock geochemistry and mineral chemistry data. *Minerals* **2023**, *13*, 1039. [[CrossRef](#)]
56. Breiter, K.; Škoda, R. Vertical zonality of fractionated granite plutons reflected in zircon chemistry: The Cínovec A-type versus the Beauvoir S-type suite. *Geol. Carpat.* **2012**, *63*, 383–398. [[CrossRef](#)]
57. Breiter, K. Monazite and zircon as major carriers of Th, U, and Y in peraluminous granites: Examples from the Bohemian Massif. *Mineral. Petrol.* **2016**, *110*, 767–785. [[CrossRef](#)]
58. Breiter, K.; Ďurišová, J.; Korblová, Z.; Lima, A.; Vašinová Galiová, M.; Hložková, M.; Dosebaba, M. Rock textures and mineral zoning—A clue to understanding rare-metal granite evolution: Argemela stock, Central-Eastern Portugal. *Lithos* **2022**, *410–411*, 106562. [[CrossRef](#)]
59. Breiter, K.; Ďurišová, J.; Korblová, Z.; Vašinová Galiová, M.; Hložková, M. Granite pluton at the Panasqueira tungsten deposit, Portugal: Genetic implications as revealed from new geochemical data. *Minerals* **2023**, *13*, 163. [[CrossRef](#)]
60. Breiter, K.; Škoda, R. Zircon and whole-rock Zr/Hf ratios as markers of the evolution of granitic magmas: Examples from the Teplice caldera (Czech Republic/Germany). *Mineral. Petrol.* **2017**, *111*, 435–457. [[CrossRef](#)]
61. Warr, L.N. IMA–CNMNC approved mineral symbols. *Mineral. Mag.* **2021**, *85*, 291–320. [[CrossRef](#)]
62. Corfu, F.; Hanchar, J.M.; Hoskin, P.W.O.; Kinny, P. Atlas of zircon textures. *Rev. Miner. Geochem.* **2003**, *53*, 469–500. [[CrossRef](#)]
63. Nasdala, L.; Kronz, A.; Wirth, R.; Váczi, T.; Pérez-Soba, C.; Willner, A.; Kennedy, A.K. The phenomenon of different electron microprobe totals in radiation-damaged and altered zircon. *Geochim. Et Cosmochim. Acta* **2009**, *73*, 1637–1650. [[CrossRef](#)]
64. Breiter, K.; Čopjaková, R.; Škoda, R. The involvement of F, CO<sup>2-</sup>, and As in the alteration of Zr-Th-REE-bearing accessory minerals in the Hora Svaté Kateřiny A-type granite, Czech Republic. *Canad. Mineral.* **2009**, *47*, 1375–1398. [[CrossRef](#)]
65. Zaraisky, G.P.; Aksyuk, A.M.; Devyatova, V.N.; Udoratina, O.V.; Chevychelov, V.Y. Zr/Hf ratio as an indicator of fractionation of rare-metal granites by the example of the Kukulbei Complex, Eastern Transbaikalia. *Petrology* **2008**, *16*, 710–736. [[CrossRef](#)]
66. Van Lichtenvelde, M.; Melcher, F.; Wirth, R. Magmatic vs. hydrothermal origins for zircon associated with tantalum mineralization in the Tanco pegmatite, Manitoba, Canada. *Amer. Mineral.* **2009**, *94*, 439–450. [[CrossRef](#)]
67. Salvi, S.; Williams-Jones, A.E. Zirconosilicate phase relation in the Strange Lake (Lac Brisson) pluton, Quebec-Labrador, Canada. *Amer. Mineral.* **1995**, *80*, 1031–1040. [[CrossRef](#)]
68. Salvi, S.; Williams-Jones, A.E. Reduced orthomagmatic C-O-H-N-NaCl fluids in the Strange Lake rare-metal granitic complex, Quebec/Labrador, Canada. *European J. Mineral.* **1992**, *4*, 1155–1174. [[CrossRef](#)]
69. Vasyukova, O.V.; Williams-Jones, A.E. Closed system fluid-mineral-mediated trace element behaviour in peralkaline rare metal pegmatites: Evidence from Strange Lake. *Chem. Geol.* **2019**, *505*, 86–99. [[CrossRef](#)]
70. Barbarin, B. A review of the relationship between granitoid types, their origins and their geodynamic environments. *Lithos* **1999**, *46*, 605–626. [[CrossRef](#)]
71. Bonin, B. A-type granites and related rocks: Evolution of a concept, problems and prospects. *Lithos* **2007**, *97*, 1–29. [[CrossRef](#)]
72. Marks, M.A.W.; Hettmann, K.; Schilling, J.; Frost, B.R.; Markl, G. The mineralogical diversity of alkaline igneous rocks. Critical factors for the transition from miaskitic to agpaitic phase assemblage. *J. Petrol.* **2011**, *52*, 439–455. [[CrossRef](#)]
73. Wood, S.A. The aqueous geochemistry of zirconium, hafnium, niobium and tantalum. *Geol. Assoc. Can. Short Course Notes* **2006**, *17*, 217–250.
74. Mikysek, P.; Zikmund, T.; Dosebaba, M.; Bříza, A.; Slobodník, M.; Adamovič, J.; Mészáros, N.; Trojek, T.; Kaiser, J. Multi-scale visualization of uranium-rich domains dispersed in U-Zr mineralization of sandstone-type (Břevniště, Czech Republic). *Ore Geol. Rev.* **2021**, *138*, 104358. [[CrossRef](#)]
75. Anders, E.; Grevesse, N. Abundances of the elements: Meteoritic and solar. *Geochim. Et Cosmochim. Acta* **1989**, *53*, 197–214. [[CrossRef](#)]

76. Barrat, J.A.; Zanda, B.; Moynier, F.; Bollinger, C.; Liorzou, C.; Bayon, G. Geochemistry of C1 chondrites: Major and trace elements, and Cu and Zn Isotopes. *Geochim. Et Cosmochim. Acta* **2012**, *83*, 79–92. [[CrossRef](#)]
77. Lyakhovich, V.V.; Shevaleevskii, I.D. Zr: Hf ratio in accessory zircons of granitoids. *Geochemistry* **1962**, 508–524.
78. Kempe, U.; Gruner, T.; Renno, A.D.; Wolf, D.; René, M. Discussion on Wang et al. (2000) Chemistry of Hf-rich zircons from the Laoshan A-type granites, Eastern China. *Mineral. Mag.* **2000**, *64*, 867–877.
79. Linnen, L.R.; Keppler, H. Melt composition control of Zr/Hf fractionation in magmatic processes. *Geochim. Et Cosmochim. Acta* **2002**, *66*, 3293–3301. [[CrossRef](#)]
80. Bau, M. Controls on the fractionation of isovalent trace elements in magmatic and aqueous systems: Evidence from Y/Ho, Zr/Hf, and lanthanide tetrad effect. *Contrib. Mineral. Petrol.* **1996**, *123*, 323–333. [[CrossRef](#)]
81. McDonough, W.F.; Sun, S. The composition of the Earth. *Chem. Geol.* **1995**, *120*, 223–253. [[CrossRef](#)]
82. Breiter, K.; Ďurišová, J.; Hrstka, T.; Korbelová, Z.; Hložková-Vaňková, M.; Vašinová Galiová, M.; Kanický, V.; Rambousek, P.; Knésl, I.; Dobeš, P.; et al. Assessment of magmatic vs. metasomatic processes in rare-metal granites: A case study of the Cínovec/Zinnwald Sn-W-Li deposit, Central Europe. *Lithos* **2017**, *292–293*, 198–217. [[CrossRef](#)]

**Disclaimer/Publisher’s Note:** The statements, opinions and data contained in all publications are solely those of the individual author(s) and contributor(s) and not of MDPI and/or the editor(s). MDPI and/or the editor(s) disclaim responsibility for any injury to people or property resulting from any ideas, methods, instructions or products referred to in the content.